ELECTROSTATIC TURBULENCE AND TRANSPORT
IN THE RFP EDGE

by

CISSE WHITE SPRAGINS

A thesis submitted in partial fulfillment of the
requirements for the degree of

Doctor of Philosophy
(Physics)

at the
University of Wisconsin-Madison
1992

ELECTROSTATIC TURBULENCE AND TRANSPORT
IN THE RFP EDGE

Cisse White Spragins
Under the supervision of Professor Stewart C. Prager
at the University of Wisconsin-Madison

ABSTRACT

This thesis details measurements of electrostatic turbulence and transport in the Madison Symmetric Torus reversed field pinch. The electrostatic fluctuation levels are found to be large, with $\tilde{n}_e / n_e \sim 30\%$ - 55% and $\tilde{T}_e / T_e \sim 15\%$ - 40%. The frequency and wavenumber spectra are broad, with $\Delta n \sim 70$ - 150 and $\Delta m \sim 3$ - 6, and differ from measured magnetic fluctuation spectra. The transport inferred from coherence measurements indicates that electrostatic fluctuations can account for most of the observed particle losses, but contribute only ~ 20% to the observed electron energy loss.

Acknowledgements

I must first acknowledge my co-worker in this project, Dr. Trudy Rempel. Without her extensive knowledge and experience with Langmuir probes, I would probably still be trying to do this experiment. I extend my deepest thanks to my advisor, Professor Stewart Prager. Through these many years, he has not only set an example as a truly first rate scientist, but as a truly first rate human being, as well. I am grateful for his patience, kindness, and helpful insight throughout this project. I am also grateful for his having put up with me, in general, which was, I am sure, no small task. I am indebted to Professor Richard Dexter for expediting my transfer into this department and for his encouragement early in my career here. Professor Clint Sprott also deserves thanks for giving me enough things to calculate, when I first joined the group, that I actually felt useful. I am honored to have had an opportunity to work with a truly great scientist, Professor Donald Kerst. I can only hope that some of his extraordinary insight into electrodynamics rubbed off. Many thanks are due to Professor Paul Terry for his part in teaching me turbulence theory, which is perhaps the most fascinating field in science which I have encountered. I would sincerely like to thank "Dr. Don" Holly for teaching me everything I know about electronics, machining, interferometry, Gravely tractors, honey bees, and anything else I didn't know just before my graduate exams. I would like to thank Dr. Mike Bevir of Culham Laboratories for what was perhaps the most enjoyable (though unfortunately brief) scientific collaboration I have had. Working with him greatly increased my insight into electrodynamics and British humo(u)r. I am indebted to Dr. Tony Leonard, whose patient help as I struggled to teach myself undergraduate physics undoubtedly contributed to my eventual understanding of it. I would also like to thank Professors Bernice and Randy Durand for their support in my endeavor to become a physicist, from being a chemist. Speaking of chemistry, I would like to thank Professor Claude Woods for his guidance and support during my time in that department. I have been much enlightened by many lectures from Professor Kirk McVoy. His brilliant insight made learning physics all the more fascinating. Lastly, I would like to thank the many plasma graduate students and members of the support staff for their assistance in making all things possible.

Unlike most physicists, I don't have a wife or girlfriend to acknowledge. However, I do have parents. I am deeply grateful for the undying and unconditional love and support from my Dad and his wife, Shelby. Through many years they refrained from asking too frequently, "When are you going to graduate?" I dedicate this thesis to my Grandmother and Grandfather. Their love and support throughout my life have been a continuous inspiration to me.

I also have a horse, Sham. I am thankful to him and to the folks at Thistle Downs for their substantial contribution to my sanity. I look

forward to spending much more time there in the near future.

Last but not least, I would like to thank Linda Van Tol for always being my friend, no matter what.

This research was financially supported by the US DOE and by the Magnetic Fusion Science Fellowship Program, administered for the US DOE by Oak Ridge Associated Universities.

Cisse W. Spragins, May 1992

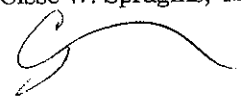

Contents

Chapter One

Introduction

Nonlinear processes in thermonuclear plasmas give rise to broadband turbulence, which manifests itself as fluctuations in observed plasma quantities, such as electric and magnetic fields, density, and fluid velocity.[1] Electrostatic fluctuations are defined as fluctuations in density, temperature, electric potential, and electric field; with the fluctuating electric field resulting from charge separation.[2] The subject matter of this work is the measurement of electrostatic fluctuations in the edge plasma of the Madison Symmetric Torus reversed field pinch.[3]

In toroidal confinement devices, such as the reversed field pinch (RFP) and the tokamak,[4] the observed cross-field particle and energy transport greatly exceeds that predicted by neoclassical diffusion theory. This observed "anomalous" transport is thought to be caused by the concurrently observed broadband turbulence, resulting from the nonlinear processes taking place within the plasma.[2,5-6] In recent years, considerable effort in tokamak research has been exerted in order to deduce the exact nature of the turbulence, in an effort to better understand the cause of the transport which leads to degradation in the particle and energy confinement times of the plasma.[7-9] Reduction in the cross-field transport currently observed in fusion devices is desirable before fusion power can become a viable, cost-effective source of energy.

The experimental study of turbulence is also of considerable interest from the point of view of basic physics.[1,10] The development of the theory of turbulence, and the theory of intensely nonlinear processes in general, are ongoing fields in modern physics with many applications outside of magnetic fusion. The study of turbulence in fusion plasmas can help extend the theory of nonlinear processes and lead to a better understanding of the basic phenomena.[11]

At the time that this work was conceived, little consideration had been given to electrostatic turbulence studies in the RFP. The primary reason for this lack of interest was due to the large (relative to the tokamak) magnetic fluctuations observed in the RFP and the consequences to the MHD equilibrium.[12] Indeed, the primary focus of RFP research had been in the attempts to understand the observed spontaneous generation of toroidal magnetic flux opposite in direction to the applied flux and the maintenance of this so-called reversal period equilibrium, hence the name RFP, for a time much longer than that predicted by resistive diffusion of the magnetic field.[13-17] This phenomenon, commonly called the dynamo for its similarity to the process of sustainment of astrophysical magnetic fields,[18] is thought to be an MHD phenomenon caused by tearing modes, manifested in large, relatively narrow-band magnetic fluctuations.[19-21] Due to this fascination with the RFP equilibrium, and indeed a reasonable need to understand the equilibrium before embarking on a study of transport, the study of electrostatic fluctuations and transport in general was

largely neglected. During this period, however, considerable research effort had been exerted in the measurement of electrostatic fluctuations and the concommitant transport in the tokamak, and early results were indicating that electrostatic turbulence could play a major role in tokamak transport.[8-10] Given these results and the similarity of the two devices, a study of electrostatic turbulence in the RFP was considered worthwhile. Since the onset of this work, studies of electrostatic fluctuation induced transport have been performed on two other RFPs.[22-23] In addition, studies of transport induced by other types of fluctuations such as magnetic, current, and velocity fluctuations have commenced on the MST and will doubtless be the subject of future theses.[24]

The scope of this work includes the measurement of temperature, density, and potential fluctuations and the computation of the resultant electostatic fluctuation induced transport. From these transport flux measurements and some assumptions about the temperature and density profiles, we estimate the plasma confinement time assuming electrostatic fluctuations are solely responsible for the transport. These measurements are made at several poloidal and toroidal locations on the machine, as well as several radial positions at one poloidal and toroidal location. The measurements are typically made at relatively low plasma current levels for the safety of the probes used to make the measurements. The basic characterization of the fluctuations in terms of the relative fluctuation levels versus radius and the mode-spectra

obtained from two-point measurements are presented in addition to the transport flux results.

We find that the relative fluctuation levels are large, with density fluctuations ranging from 30% to 55%, and temperature fluctuations ranging from 15% to 40%. The frequency and wave-number spectra are broad, with Δn ~ 70 - 150 and Δm ~ 3 - 6, and differ from measured magnetic fluctuation spectra. The transport inferred from coherence measurements indicates that electrostatic fluctuations can account for most of the observed particle losses, but contribute only ~ 20% to energy loss.

The organization of the thesis is as follows. Chapter Two covers the relevant transport equations and gives a survey of previous experimental work in the field of electrostatic fluctuations. Chapter Three provides a brief overview of RFP's in general. In addition, a description of MST, the machine on which the experiments were performed, is provided. This description includes a brief physical description, a description of the magnetic field system, the plasma parameters, and diagnostics. The emphasis is on those features of the machine which are specifically relevant to the work presented here. Chapter Four presents an overview of simple probe theory and the corrections to that theory which are used, as well as a description of the experimental setup, including probes, electronics, and data acquisition. In addition, the exact definitions of the statistical quantities contained in the transport equations and the explicit methods of calculation, are presented. The actual experimental results are presented in Chapter

Five and the final chapter summarizes the results and conclusions.

As a final note, the calculation of transport is carried out in SI units. However, quantities will often be expressed in terms of other units, if they are the more commonly used ones in plasma physics, eg. density is expressed in units of inverse cubic centimeters and temperature in units of electron volts. Boltzmann's constant and the electrostatic charge are not used in expressions, eg. "$e\Phi$ / kT" is written simply as "Φ / T"; temperature assumes the unit of volts in expressions which also involve potential.

References

1 B. B. Kadomtsev, *Plasma Turbulence*, Academic Press, London (1965).

2 P. C. Liewer, Nucl. Fusion **25**, 543 (1985).

3 R. N. Dexter *et al.*, Fusion Tech. **19**, 131 (1991).

4 L. Artsimovich, Nucl. Fusion **12**, 215 (1972).

5 *Status of Tokamak Research*, J. M. Rawls, ed., U. S. DOE, Washington, D. C. DOE/ER-0034 (1979).

6 J. Hugill, Nucl. Fusion **23**, 331 (1983).

7 Ch. P. Ritz, R. D. Bengtson, S. J. Levinson, E. J. Powers, Phys. Fluids **27**, 2956 (1984).

8 S. Zweben, P. C. Liewer, R. W. Gould, J. Nucl. Mater. **111** & **112**, 39 (1982).

9 S. J. Levinson, J. M. Beall, E. J. Powers, R. D. Bengtson, Nucl. Fusion **24**, 527 (1984).

10 S. A. Orzag, J. Fluid Mech. **41**, 363 (1970).

11 A. Hasegawa and K. Mima, Phys. Fluids **21**(1), 87 (1978).

12 H. A. B. Bodin and A. A. Newton, Nucl. Fusion **20**, 1255 (1980).

13 E. J. Caramana, R. A. Nebel, and D. D. Schnack, Phys. Fluids **26**, 1305 (1983).

14 R. G. Watt and R. A. Nebel, Phys. Fluids **26**, 1168 (1983).

15 D. D. Schnack, E. J. Caramana, and R. A. Nebel, Phys. Fluids **28**, 321 (1985).

16 A. Y. Aydemir and D. C. Barnes, Phys. Rev. Lett. **52**, 930 (1984).

17 A. Y. Aydemir, D. C. Barnes, E. J. Caramana, A. A. Mirin, R. A. Nebel, D. D. Schnack, and A. G. Sgro, Phys. Fluids **28**, 898 (1985).

18 H. K. Moffatt, *Magnetic Field Generation in Electrically Conducting Fluids*, Cambridge Univ. Press, 104 (1978).

19 H. R. Strauss, Phys. Fluids **27**, 2580 (1984).

20 H. R. Strauss, Phys. Fluids **28**, 2786 (1985).

21 Z. G. An, P. H. Diamond, R. D. Hazeltine, J. N. Leboeuf, B. A. Carraras, L. Garcia, T. C. Hender, H. R. Hicks, J. A. Holmes, V. E. Lynch, and H. R. Strauss, in *Plasma Physics and Controlled Nuclear Fusion Research*, (Proc. of the Tenth Int. Conf. ,London, 1984) Vol. II, IAEA, Vienna, 231 (1985).

22 H. Ji, H. Toyama, K. Miyamoto, S. Shinohara, and A. Fujisawa, Phys. Rev. Lett. **67**, 62 (1991).

23 H. Y. W. Tsui *et al.*, Nucl. Fusion **31**, 2371 (1991).

24 W. Shen, R. N. Dexter, and S. C. Prager, Phys. Rev. Lett. **68**, 1319 (1992).

Chapter Two

Background

A. Transport Equations

Before launching into a survey of previous and concurrent experimental work in this field, an overview of the quantities measured and the equations relating them to the specific quantities of interest for transport will be presented. This overview will be brief and contain only the critical information necessary for the reader to appreciate the results that follow. A very detailed description of the equations and the explicit methods of calculation will be presented in Chapter Four.

A convection of particles, perpendicular to the applied magnetic field, due to electrostatic fluctuations is defined as:[1]

$$\Gamma_p = \langle \tilde{n}_e \tilde{v}_r \rangle \tag{2.1}$$

where $\langle\,\rangle$ denotes an ensemble average and $\tilde{n}_e, \tilde{v}_r$ denote fluctuating electron density and radial velocity respectively. This quantity is proportional to the squared coherence (linear relationship) between $\tilde{n}_e$ and $\tilde{v}_r$. The fluctuating velocity, $\tilde{\mathbf{v}}$, is given by:

$$\tilde{\mathbf{v}} = \frac{\tilde{\mathbf{E}} \times \mathbf{B}}{B^2} \tag{2.2}$$

the fluctuating $\mathbf{E}\times\mathbf{B}$ drift velocity.

Similarly, electron energy transport due to electrostatic fluctuations

is given by:[2]

$$\Gamma_E = \frac{3}{2} \langle \tilde{p}_e \tilde{v}_r \rangle \tag{2.3}$$

where $\tilde{p}_e$ is the fluctuating pressure given by:

$$\tilde{p}_e = n_e \tilde{T}_e + \tilde{n}_e T_e \tag{2.4}$$

where T_e is the electron temperature. Clearly, care must be taken using such an equation, since the relative phase of the fluctuations in n_e and T_e is important, in addition to the amplitudes. The term proportional to $\tilde{T}_e\tilde{v}_r$ is the conductive part of the electron energy transport, and the term proportional to $\tilde{n}_e \tilde{v}_r$ is the convective part. Assuming quasineutrality, the convective ion energy transport would be equal to that for electron energy. In order to obtain the conductive part, however, a measurement of $\tilde{T}_i$ would be needed. Ion temperature fluctuations are not measured in the work presented here.

Typically, measurements of these quantities in the edge are made using electrostatic (Langmuir) probes. A conducting wire placed in the plasma and biased negatively to several times the the local electron temperature will draw ion saturation current, J_{sat}, where $J_{sat} \propto n\sqrt{T_e}$, according to simple probe theory.[3] For fluctuating quantities, with $\tilde{T}_e / T_e << 1$, expansion gives:

$$\frac{\tilde{J}_{sat}}{J_{sat}} \approx \frac{\tilde{n}}{n} + \frac{1}{2}\frac{\tilde{T}_e}{T_e} \tag{2.5}$$

Again, the relative phases of $\tilde{n}$ and $\tilde{T}_e$ are important as well as the amplitudes.

Measurements of $\tilde{E}$ are made by measuring the potential of two closely spaced probes and calculating the gradient by $\tilde{E} = -ik\tilde{\Phi}$. An

isolated probe placed in the plasma will measure floating potential, however, the gradient of the plasma potential is needed for transport:[3]

$$\Phi_{plasma} = \Phi_{float} - \alpha T_e \qquad (2.6)$$

and analogously for the the fluctuating quantities:

$$\tilde{\Phi}_{plasma} = \tilde{\Phi}_{float} - \alpha \tilde{T}_e \qquad (2.7)$$

where α is the electron temperature normalized sheath drop (a negative constant with the sign convention used here). Again, the relative phase of $\tilde{\Phi}_{float}$ and $\tilde{T}_e$ is of critical importance.

If $\tilde{T}_e / T_e << \tilde{n} / n$ then, from equations 2.5 and 2.7, $\tilde{n} / n \sim \tilde{J}_{sat} / J_{sat}$ and $\tilde{\Phi}_{plasma} \sim \tilde{\Phi}_{float}$ which simplifies matters considerably, as no measurement of $\tilde{T}_e$ must be made. In this instance then, the energy transport is purely convective and only the $\langle \tilde{n}_e \tilde{v}_r \rangle$ term contributes, where $\tilde{n} / n \equiv \tilde{J}_{sat} / J_{sat}$.

If the temperature fluctuations are significant, then they are typically measured by the triple probe technique,[4] which gives equilibrium and fluctuating values of T_e. This method consists of an ion saturation current double probe in combination with a probe measuring floating potential. In practice, this measurement is less reliable than the individual measurements of floating potential and ion saturation current.

B. Previous Experimental Work

1. Zeta

Some of the earliest observations of electrostatic fluctuations in fusion plasmas and their relation to transport were made on the Zeta device at Culham Laboratory in England in the mid 1960s.[5] Zeta[6] was a large (R=1.5m, a=0.5m) experimental magnetic fusion machine, which was the first to be operated as what is now known as a reversed field pinch. The device was similar in size to MST[7] and, like MST, was surrounded by a thick conducting wall. The poloidal field was coupled through a large, 7 volt-second iron core (as opposed to 2 volt-seconds for MST). Although the two devices bear major similarities, MST is a longer pulse length, longer confinement time device. A major reason for this difference is probably due to the significantly lower magnetic field errors exhibited in MST, a property to which RFP's are well known to be particularly sensitive.

The properties of electrostatic fluctuations in Zeta were all deduced from the measurement of the current to a double probe and its rms fluctuation level, versus bias voltage. Through analytical and numerical analysis of these data curves, invoking simple probe theory, estimates of n, T_e, and E and their corresponding fluctuation levels were made. A lower-bound estimate of the electrostatic fluctuation induced transport, from the $\langle \tilde{n}_e \tilde{v}_r \rangle$ term, was also made. Although the methods

employed were rather indirect by today's standards,[8] they represent a clever usage of the available technology. Even without the computer-data-acquisition capability that is now relied upon so heavily, the experimenters were able to obtain an estimate of some of the quantities of interest.

In 150 kA, cool plasmas, the experimenters were able to insert probes well into the plasma to obtain the density and temperature profiles shown in Figure 2.1. As is shown in the graphs, the profiles are relatively flat in the central portion of the plasma and drop rather steeply in the edge region. Although there is very little profile

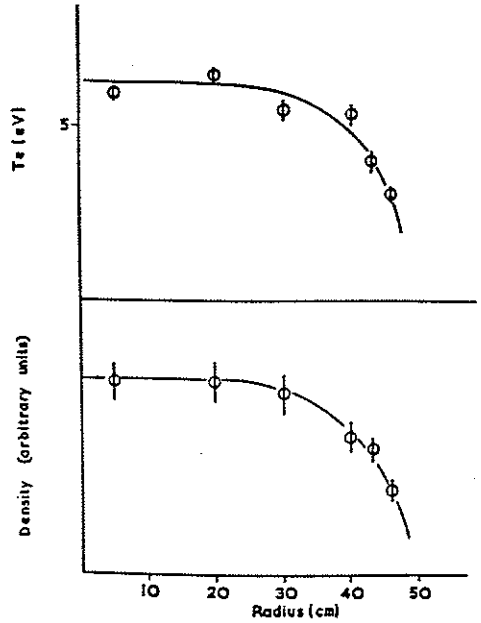

Figure 2.1--Density and electron temperature profiles in Zeta (from Reference 5).

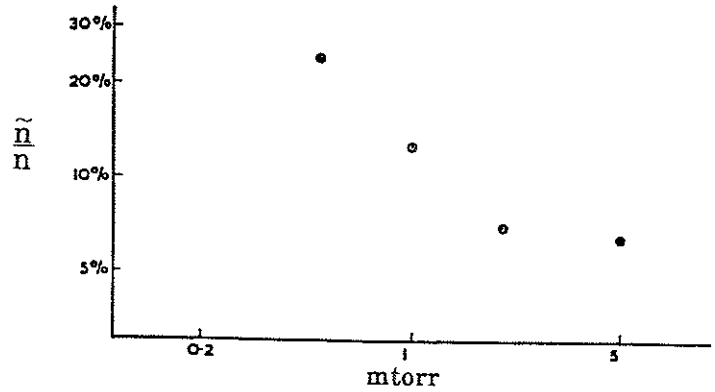

Figure 2.2--Relative density fluctuation levels versus fill pressure in Zeta (from Reference 5).

information available from present-day RFPs, current indications suggest that their profiles are indeed quite similar to those observed on Zeta.

As is shown in Figure 2.2, the relative density fluctuatation leveldecreases with increasing fill pressure, with $\tilde{n}/n$ ranging from 6 to 24%. These relative fluctuation levels are somewhat smaller than those seen in present day RFPs.[9-11]

The r.m.s. fluctuation levels of density and electric field versus radius are shown in Figure 2.3. Although the r.m.s. fluctuation levels decrease, particularly in the case of density in the edge region, the relative fluctuation levels increase in the edge region.

Overall, the observed probe current fluctuations were found to be

principally due to density fluctuations, although temperature fluctuations were not negligible at high pressures. In the case of negligible temperature fluctuations, an estimate of $\langle \tilde{n}_e \tilde{v}_r \rangle$ yielded a particle confinement time on the order of that measured by other means.

Although the methods used in the Zeta work had some technological limitations, it is interesting that many of the observations agree, at least qualitatively, with those made recently.

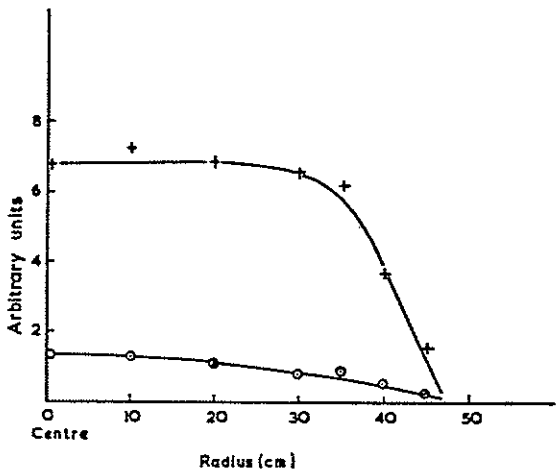

Figure 2.3--R.M.S. density (+) and electric field (O) fluctuations versus radius in Zeta (from Reference 5).

2. Cal-Tech Research Tokamak

The first work to be conducted which used modern computational methods similar to those of the present work, was performed on the Cal-Tech Research Tokamak ($R = 45$ cm, $a = 15$ cm, $B_T = 4$ kG, $T_{e0} \cong 100$ eV, $n_{e0} \sim 10^{12} - 10^{13}$ cm^{-3}).[12]

The edge plasma was found to have $n(\text{edge}) \approx 0.5 - 5 \times 10^{12}$ cm^{-3}, $T_e(\text{edge}) \cong 25$ eV, along with a large level of broadband density and potential fluctuations, $\tilde{n}/n \approx \tilde{\Phi}/T \approx 10\% - 50\%$. The edge measurements were performed using a three-tip Langmuir probe, in which one tip operated as a single-tip J_{sat} probe and the remaining two tips measured floating potential (and hence its gradient). The experimenters assumed the temperature fluctuations to be negligible; an assumption which was somewhat substantiated by evidence from other tokamaks.

The fluctuations were found to be broadband and decreasing with frequency. The phase between $\tilde{n}$ and $\tilde{E}$ was found to be within $0 \pm 60°$ for frequencies less than 500 kHz, yielding a particle flux of 10^{17} particles / cm^{2}s with the major contribution coming from the frequency components below 200 kHz. Assuming poloidal and toroidal symmetry, this flux yields $\tau_p \sim \tau_E \sim 1$ ms, which is of the same order as the observed particle and energy confinement times. These results, which are shown in Figure 2.4, bear at least a qualitative resemblance to the results of the present work.

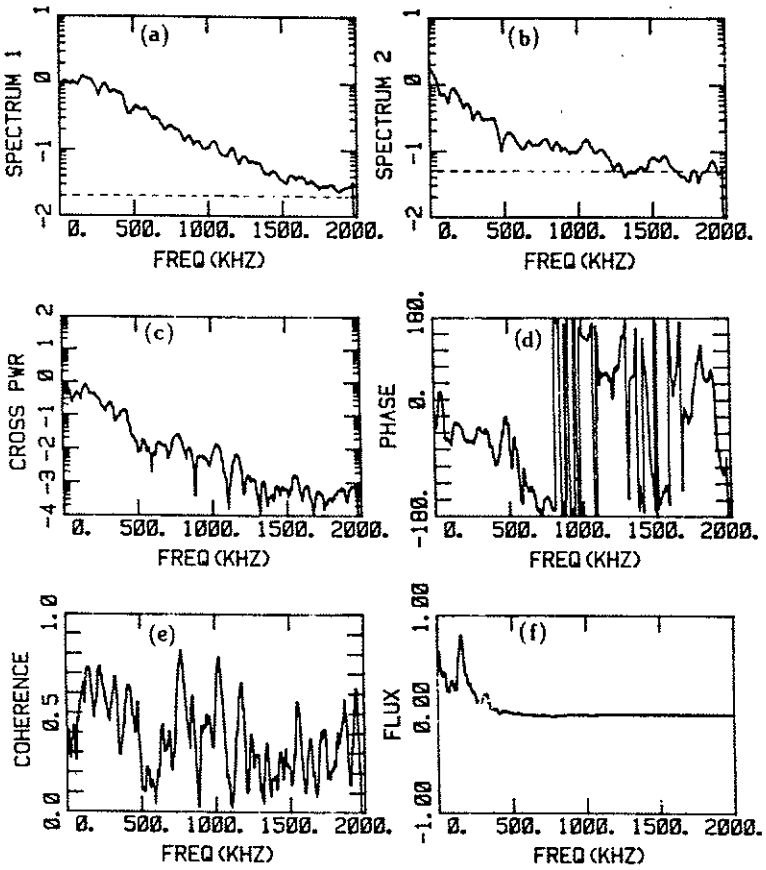

Figure 2.4-- (a) amplitude spectrum of $\nabla\tilde{\Phi}_f$ *; (b) amplitude spectrum of* $\tilde{n}$ *; (c) cross-power spectrum of* $(\nabla\tilde{\Phi}_f, \tilde{n})$ *; (d) phase between* $\nabla\tilde{\Phi}_f$ *and* $\tilde{n}$ *(degrees) ; (e) coherence between* $\nabla\tilde{\Phi}_f$ *and* $\tilde{n}$ *; and (f) radial flux (from Reference 12).*

3. PreTEXT and TEXT

Perhaps the most comprehensive study of electrostatic fluctuations in the tokamak was begun on PreTEXT and later continued on TEXT at the University of Texas at Austin Fusion Research Center.

In PreTEXT (a=14 cm, R=53.3 cm) plasmas with I_p= 40 kA, T_e= 200 eV, $\bar{n} = 5 \times 10^{12}$ cm^{-3}, and 50 msec duration, the experimenters found $T_{e,\ edge} \approx 20$ eV with quite a flat profile.[13] The density and floating potential profiles were, on the other hand, found to be quite steep in the edge. These results are shown below in Figure 2.5.

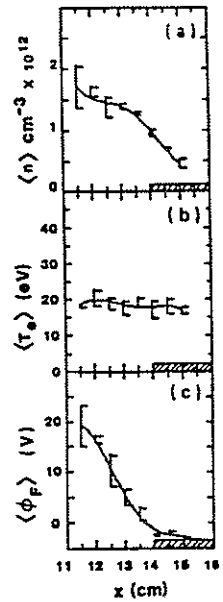

Figure (2.5) -- Radial profiles of time-averaged data shown for: (a) ion density, (b) electron temperature, and (c) floating potential. The limiter is located at x=14 cm (from Reference 13)

As in the Cal-Tech work discussed previously, the temperature fluctuations were again taken to be negligible in this work as well. The density fluctuation profile was higher in the edge and decreases farther into the plasma, while the potential fluctuation profile assumed the opposite trend. This phenomenon caused the plasma to appear to be Boltzmann only within a narrow radial range near the limiter edge. These results are shown below in Figure 2.6.

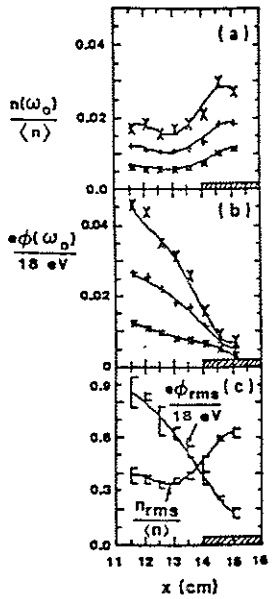

*Figure 2.6 -- Fluctuation profiles for individual frequency components: × 20 kHz, + 50 kHz, * 100 kHz, shown for: (a)* $n(\omega_0)/\langle n\rangle$ *and (b)* $e\Phi(\omega_0)/T_e$. *In (c) the rms values of* $\tilde{n}/n$ *and* $e\tilde{\Phi}/T_e$ *reveal a strikingly different scaling with minor radius (from Reference 13).*

In a highly nonlinear system such as a turbulent plasma, a deterministic relationship between frequency and wavenumber (dispersion relation) does not exist. A useful statistical description of the turbulence, however, is provided by the wavenumber/frequency spectrum $S(k,\omega)$, which describes the power spectrum of the turbulence as a function of both the frequency and wavenumber.[14] The details of the calculation of this quantity will be covered in Chapter Four. Measurements of $S(k,\omega)$ for both density and potential fluctuations in PreTEXT show the wavenumber spectrum to be considerably more narrow in the toroidal direction than the poloidal direction.

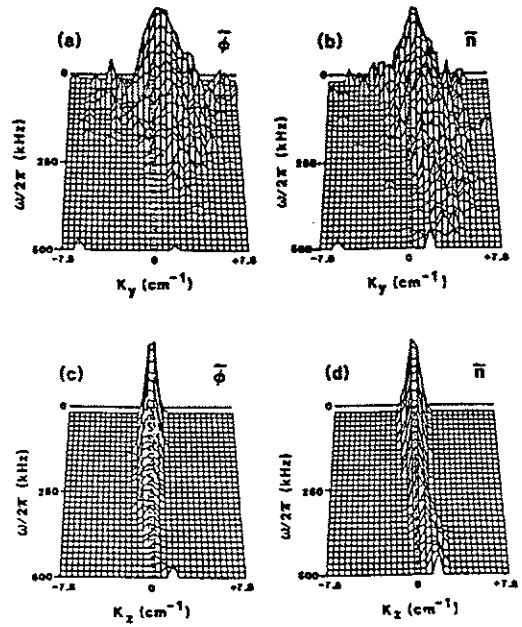

Figure 2.7 -- (a) $S(k_y,\omega)$ *for* Φ *, (b)* $S(k_y,\omega)$ *for* $\tilde{n}$ *, (c)* $S(k_z,\omega)$ *for* $\tilde{\Phi}$*, (d)* $S(k_z,\omega)$ *for* $\tilde{n}$ ($\hat{y}$ *is poloidal and* $\hat{z}$ *is toroidal) (from Reference 13).*

This observation is not surprising since the fluctuations along the direction of the magnetic field would be expected to be of much longer wavelength than those transverse to the magnetic field. These results are shown above in Figure 2.7.

The coherence between $\tilde{n}$ and $\tilde{\Phi}$ was found to have an amplitude of about 0.6 and decreasing with frequency, while the relative phase of the fluctuations was found to be close to 90°. From the coherence, the particle transport flux was obtained as a function of minor radius. From this flux, a particle confinement time of approximately 2 msec was estimated, which agrees well with estimates from spectroscopic data. The energy confinement time for the same shots is about four times lower, however. A plot of the particle flux as a function of minor radius is shown below, which shows a decrease in flux near the edge region.

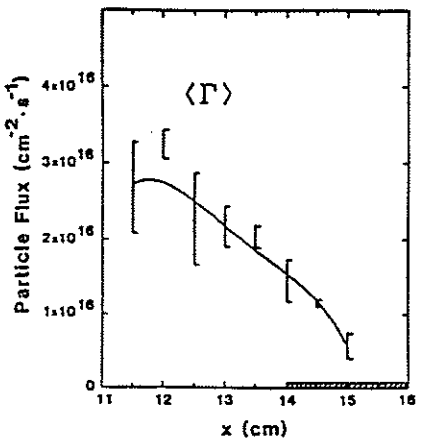

Figure 2.8 -- Electrostatic fluctuation induced particle flux as a function of minor radius (from Reference 13).

Similar electrostatic fluctuation research has also been conducted on the TEXT tokamak (R=1m, a=0.27m).[15] The experiments were conducted in 200 kA plasmas with $n_e = 4 \times 10^{13}$ cm^{-3}, $T_{eo} = 800$ eV, and $\tau_p = 8$ msec. The properties of the edge electrostatic fluctuations in TEXT are shown in Figures 2.9-2.13. The most noticeable feature of the spatial variations in the fluctuations is the presence of a shear layer, a radially extended region in which the phase velocity changes from one direction to the other. The shear layer is attributed to a radial variation in the direction of the electric field. The ensemble-averaged k-spectrum shown in Figure 2.9 demonstrates the change in phase velocity from the ion drift direction on the large minor radius of the shear layer to the electron drift direction on the small minor radius side. Density and potential fluctuations are shown in Figure 2.10. For all the discharges studied in TEXT, $\tilde{n} / n < \tilde{\Phi} / T_e$ for radii less than that of the limiter. As is shown in Figure 2.11, the phase angle between n and Φ is close to 90°. The spectrum of $\Gamma(\omega)$ is shown in Figure 2.12 for three radial positions, each indicating that the primary contributions come from the frequency components below 200kHz. The radial variation of the particle flux is shown in Figure 2.13, which indicates the minimum in the shear layer region. The maxima in the flux correspond to the maxima in the density and potential fluctuations. A comparison of the global particle confinement time with that derived from electrostatic transport is shown in Figure 2.14, for various line-averaged electron densities. The values agree reasonably well at all densities and scale in the same way;

therefore, electrostatic fluctuations would appear to account for most of the transport in the plasma edge.

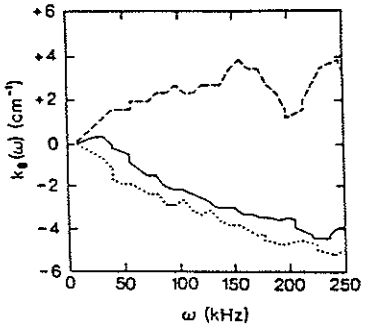

Figure 2.9 -- Ensemble-averaged poloidal wavenumber spectra at three radial positions: r=24.9 cm (--), r=26.4 cm (__), r=27.3 cm (···) (from Reference 15).

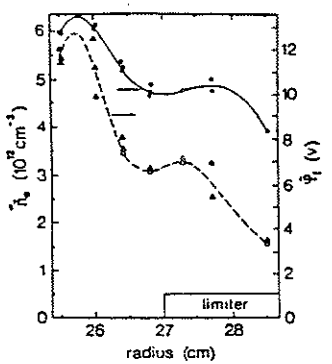

Figure 2.10 -- Spatial variation of density and potential fluctuations (from Reference 15).

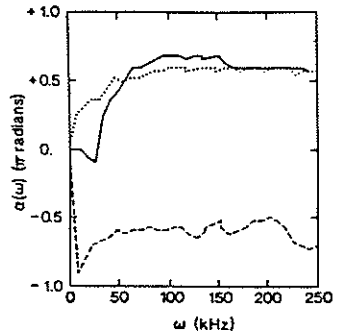

Figure 2.11 -- Phase angle between n and Φ for the same radial positions as Figure 2.9 (from Reference 15).

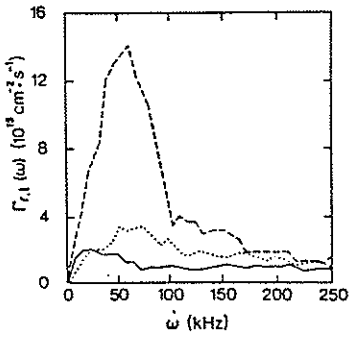

Figure 2.12 -- Γ(ω) due to electrostatic fluctuations, at the same radial positions as Figure 2.9 (from Reference 15).

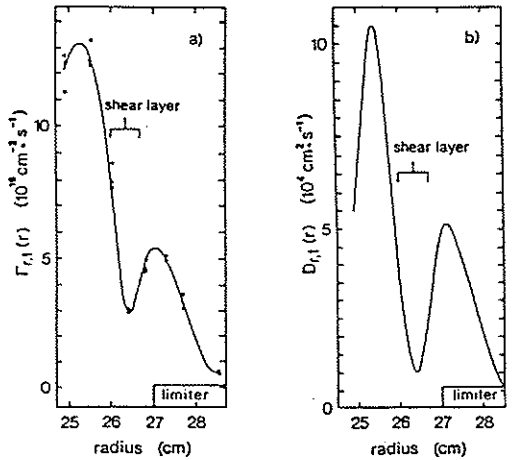

Figure 2.13 -- Radial particle flux (a), and diffusion coefficient (b), due to electrostatic fluctuations, versus radius (from Reference 15).

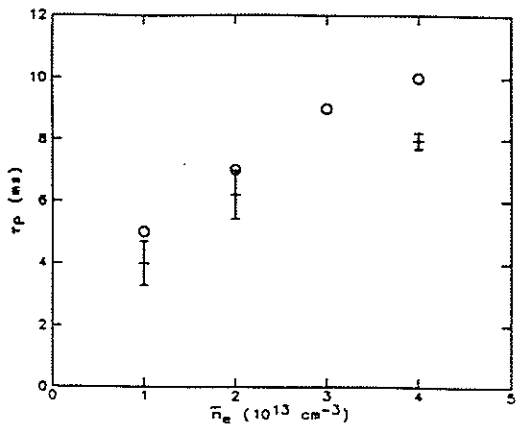

Figure 2.14 -- Global particle confinement time (+) and confinement time predicted from electrostatic fluctuations measurements (o) versus line-averaged electron density (from Reference 15).

C. Concurrent RFP Work

1. REPUTE-1

Recent studies of electrostatic fluctuations in the RFP have been performed on REPUTE-1 (R=82 cm, a=22 cm, I_p=110 kA, $\tau_p \sim 40$ μsec).[10] The experimenters used a movable probe to make measurements from r=a/2 to r=a. The probe used in the experiment consisted of six tips, with two tips operating as a J_{sat} double probe and the remaining four tips measuring floating potential with both poloidal and toroidal separation, in order to calculate both E_{tor} and E_{pol}.

Unlike the assumptions made in the tokamak work, the temperature fluctuations in the RFP were measured and found to be substantial; therefore, they cannot be disregarded in the calculation of fluxes. The mean and fluctuating quantities versus radius are shown in Figure 2.15. (The experimenters also measured magnetic fluctuations which are shown as well.)

The electrostatic fluctuation induced electron heat transport can be shown to be a sum of four terms with the contributions of $\tilde{n}$ and $\tilde{T}_e$, and $\tilde{E}_{pol}$ and $\tilde{E}_{tor}$ separated. A plot of these individual terms and their sum are shown versus radius in Figure 2.16. The results indicate that while $\tilde{E}$ and $\tilde{T}_e$ are almost in phase, they are in antiphase with $\tilde{n}$. Since the magnitudes of $\tilde{n}/n$ and $\tilde{T}_e/T_e$ are comparable and they are in antiphase, their results on the overall energy flux cancel. Not only do

the contributions from the individual terms cancel, the terms themselves are small, as well. The particle flux does not depend on $\tilde{T}_e$,

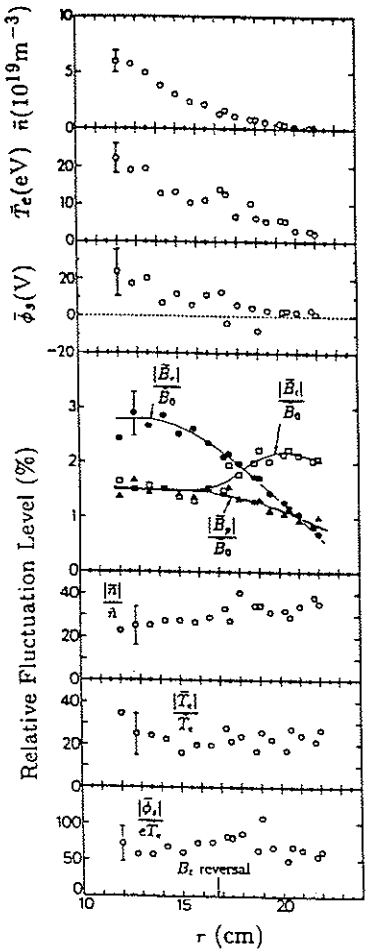

Figure 2.17 -- Radial profiles of the mean values and relative fluctuation levels of the density, electron temperature, plasma potential, and magnetic field (from Reference 10).

however; therefore, in the interior region of the plasma, the electrostatic fluctuation induced particle flux can account for roughly one third of the overall particle flux.

Although these results are interesting, the plasmas on which they were conducted do not represent the optimum RFP performance. REPUTE-1[16] has very large field errors due primarily to the large portholes in the conducting shell. These errors manifest themselves in the large loop voltages observed (~220 V). Also, the values of the field reversal parameter F, and the pinch parameter Θ, of ~-0.4 and ~2.0 respectively, are quite far from the standard parameters predicted by the Modified Bessel Function Model,[17] which describes most RFPs quite well. Given these considerations, it is not obvious that these results would apply to RFPs in general.

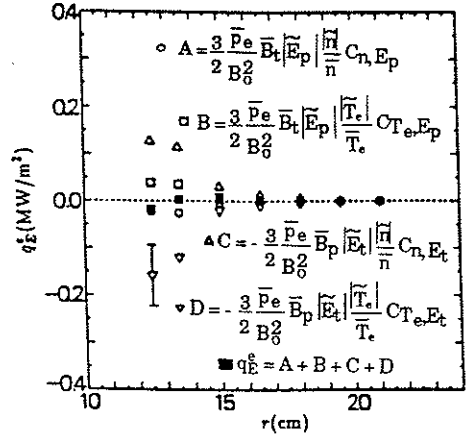

Figure 2.18 -- Radial profiles of the electrostatic fluctuation induced electron heat flux expressed as a sum of four terms (from Reference 10).

2. ZT40M

Electrostatic fluctuations have been measured in the edge of the ZT40M RFP (R=1.14 m, a=0.2 m). As in the present experiment, the fluctuation levels are large, with $\tilde{n}_e / n_e \sim 40\%$ and $\tilde{T}_e / T_e \sim 50\%$. The experimenters find that beyond the shadow of a movable graphite limiter, the electrostatic fluctuation induced particle flux is comparable to the global particle flux estimated by other means. In the limiter shadow, however, there is a 60% reduction in the particle flux, with the primary reduction occuring in the low frequency (< 50 kHz) components. These results are shown below, in Figure 2.19.

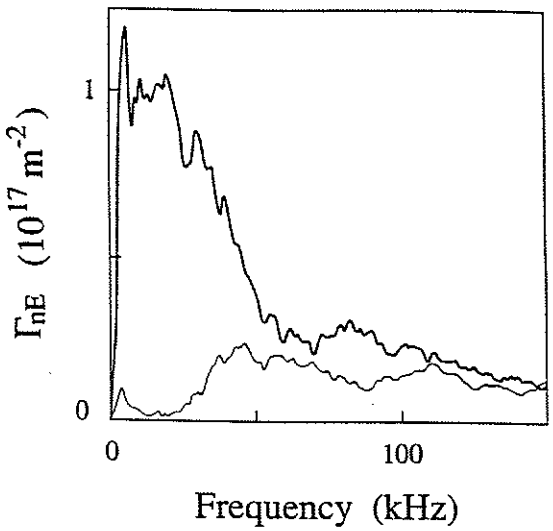

Figure 2.19 -- Particle flux in the edge region, beyond the limiter (darker line) and behind the limiter (lighter line) (from Reference 11).

In both regions, however, the electrostatic fluctuation induced energy flux is small compared to the global energy flux measured by other means. These results bear similarities to those obtained on MST in the present experiment. In contrast to our results, the correlation between electrostatic and magnetic fluctuations is found to be quite high in ZT40M, particularly at low frequencies (< 50 kHz), where the MHD activity is strongest. This result is shown below in Figure 2.20.

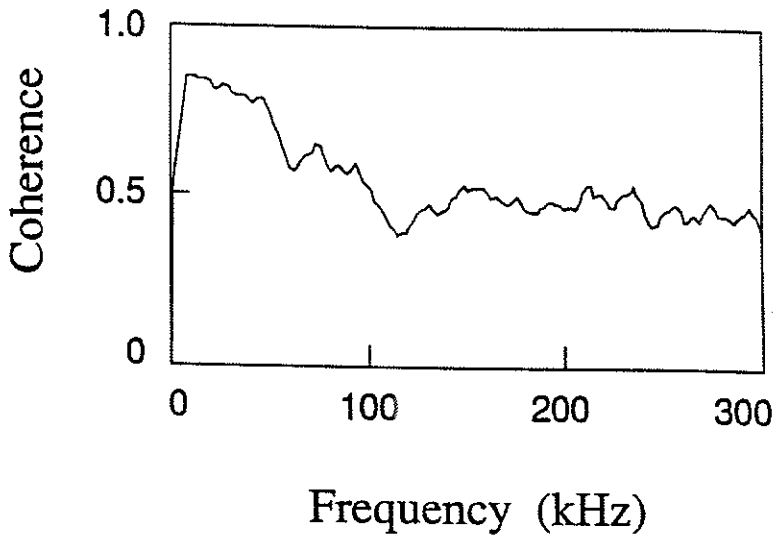

Figure 2.20 -- Coherence between ion saturation current fluctuations and radial magnetic field fluctuations (from Reference 11).

The experimenters, in fact, maintain that the electrostatic fluctuation activity below 50 kHz is primarily attributable to the coupling of MHD activities to the equilibrium gradients through ideal flux surface perturbations. This supposition appears not to be the case in MST, as is illustrated in Figure 5.6.

References

1 E. J. Powers, Nuclear Fusion **14**, 794 (1974).

2 P. C. Liewer, J. M. Mc Chesney, S. J. Zweben, and R. W. Gould, Phys. Fluids **29**, 309 (1986).

3 F. F. Chen, in *Plasma Diagnostic Techniques*, Academic Press, New York 113 (1965).

4 S. L. Chen, T. Sekiguchi, J. Applied Phys. **36**, 2363 (1965).

5 D. C. Robinson and M. G. Rusbridge, Plasma Physics **11**, 73 (1965).

6 D. C. Robinson et al, 2nd European Conference on Controlled Fusion and Plasma Physics, Stockholm (1967).

7 See Chapter Three, this thesis.

8 Ch. P. Ritz et al., Rev. Sci. Instr. **59**, 1735 (1988).

9 See Chapter Five, this thesis.

10 H. Ji, H. Toyama, K. Miyamoto, S. Shinohara, and A. Fujisawa, Phys. Rev. Lett. **67**(1), 62 (1991).

11 H. Y. W. Tsui *et al.*, Nucl. Fusion **31**, 2371 (1991).

12 S. Zweben, P. C. Liewer, and R. W. Gould, J. Nucl. Mat. **111**, 39 (1982).

13 S. J. Levinson, J. M. Beall, E. J. Powers, R. D. Bengtson, Nucl. Fusion **24**, 527 (1984).

14 J. M. Beall, Y. C. Kim, E. J. Powers, J. Appl. Phys. **43**, 3993 (1982).

15 W. L. Rowan, C. C. Klepper, C. P. Ritz, R. D. Bengtson, K. W. Gentle, P. E. Phillips, T. L. Rhodes, B. Richards, A. J. Wootton, Nucl. Fusion **27**(7), 1105 (1987).

16 N. Askura et al, Nucl. Fusion **29**, 893 (1989).

17 K. F. Schoenberg, R. F. Gribble, and J. A. Phillips, Nucl. Fusion **22**, 1433 (1982).

Chapter Three

Machine Description

The Madison Symmetric Torus (MST)[1] is the machine on which the experiments in this thesis were performed. It is of the type known as a reversed field pinch (RFP). The RFP is a toroidal confinement device which is similar in some respects to the tokamak. There are considerable differences, however. The RFP equilibrium is a minimum energy state in which the magnetic fields are reasonably well described by a model known as the Bessel Function Model (BFM).[2,3] In this model, the magnetic fields are solutions of $\nabla \times \mathbf{B} = \lambda \mathbf{B}$ where λ is a constant. Assuming constant pressure and cylindrical symmetry, the fields are given by: $B_t = B_0 J_0(\lambda r)$, $B_p = B_0 J_1(\lambda r)$, $B_r = 0$; where B_t is the toroidal field, B_p is the poloidal field, B_r is the radial field, B_0 is the on-axis magnetic field, and J_0 and J_1 are Bessel functions. This model is based on the conservation of global (but not local) magnetic helicity. The magnetic field profiles are shown in Figure 3.1. As is shown in the graph, the toroidal magnetic field in the edge actually reverses direction, hence the name RFP. This reversal is produced spontaneously in the plasma and is a manifestation of the relaxed state. The phenomenon that generates this relaxed state is known as the "dynamo effect"[4] for its similarity to the process by which astrophysical magnetic fields[5] are sustained for times much longer than that

predicted by resistive diffusion. In the same way, in an RFP the self-generated toroidal flux[6] is sustained for a time longer than that predicted by resistive diffusion. The dynamo effect is widely thought to be an MHD phenomenon generated by global tearing modes.

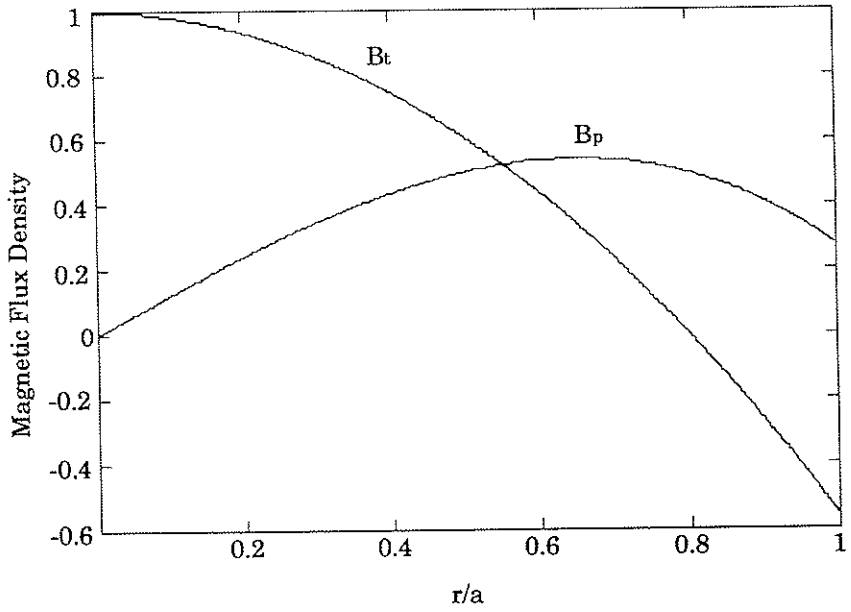

Figure 3.1 -- Magnetic field profiles in the RFP as predicted by the Bessel Function Model.

One perhaps unfortunate manifestation of the RFP equilibrium is that the plasma performance is very sensitive to edge conditions and is detrimentally affected by magnetic field errors[7,8] in the edge such as

those caused by portholes and non-ideal magnetic field winding placement. Also, the equilibrium requires a close fitting, thick, conducting shell for stability,[9] where thick means that the time constant for vertical field penetration is long compared to the pulse length.

Due to these considerations, MST was constructed to minimize the magnetic field errors and to have the conducting shell as close to the plasma as possible. Two views of the machine are shown in Figures 3.2 and 3.3.

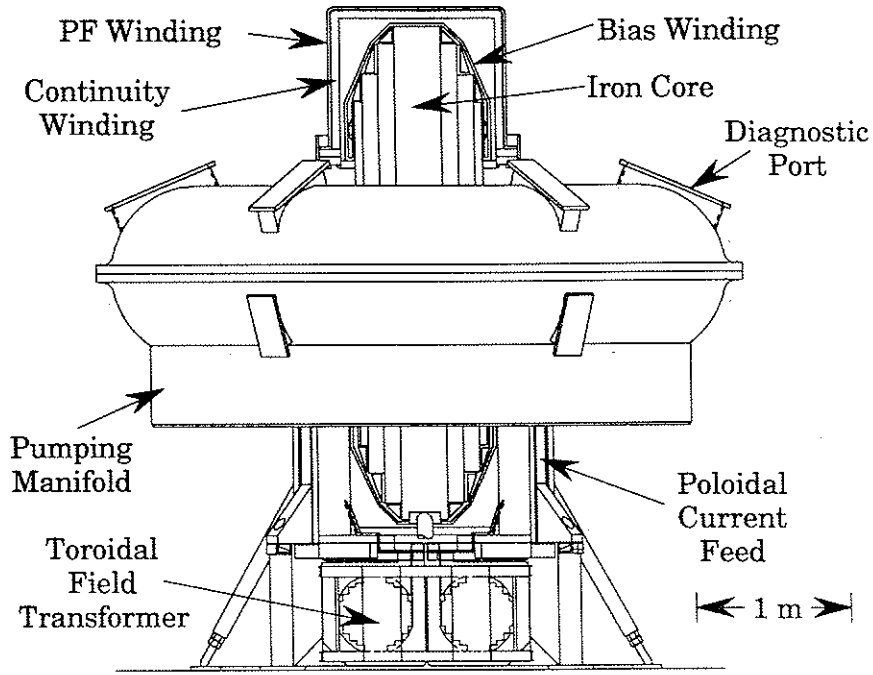

Figure 3.2-- MST - East View

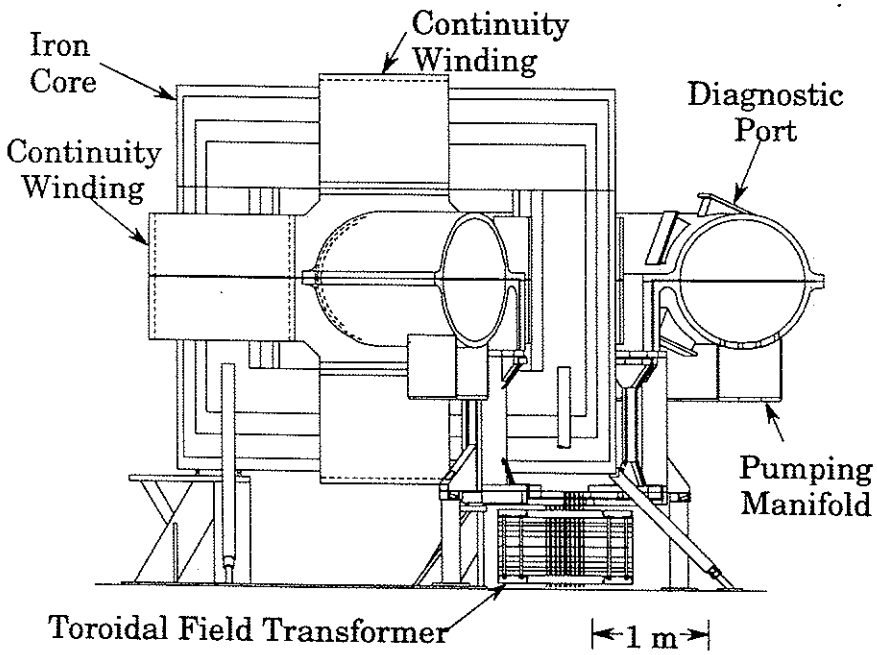

Figure 3.3 -- MST - South View

A 5 cm thick toroidal aluminum vessel serves as the vacuum vessel, the stabilizing shell, the plasma first wall, and the toroidal field winding. The toroid is in two halves with the cut at the equatorial plane. The inner toroidal gap is insulated and the outer gap is conducting (Figure 3.4). The current for the toroidal field travels up through four transmission lines which connect to an inner feed cylinder which then spreads the current flow out toroidally. The current is then driven through the vessel wall poloidally due to the inner insulated gap. This

current then produces the toroidal field. This design eliminates the field ripple which would be caused by discrete windings.

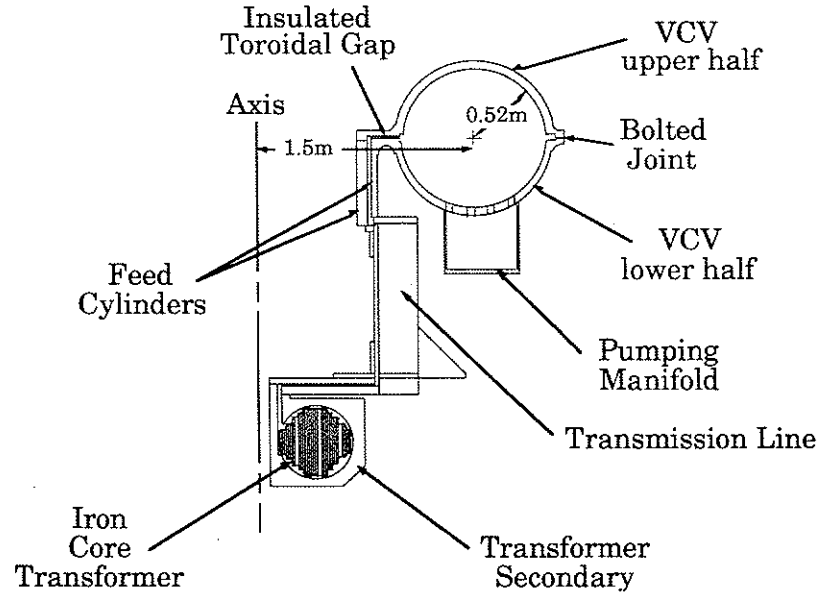

Figure 3.4 -- MST Toroidal Field System

The poloidal field system (Figure 3.5) consists of a forty-eight ton iron core in which one leg goes through the center hole of the torus. The core is wound with the poloidal field winding which is the primary of the transformer. The plasma itself acts as the secondary of the transformer. The induced toroidal plasma current then creates the poloidal magnetic field. There is a poloidal cut in the vacuum containment vessel (VCV) at the same toroidal location as the iron core

which prevents the vessel from linking the core. The poloidal field windings are placed in such a way as to reduce the field errors caused by the poloidal cut.

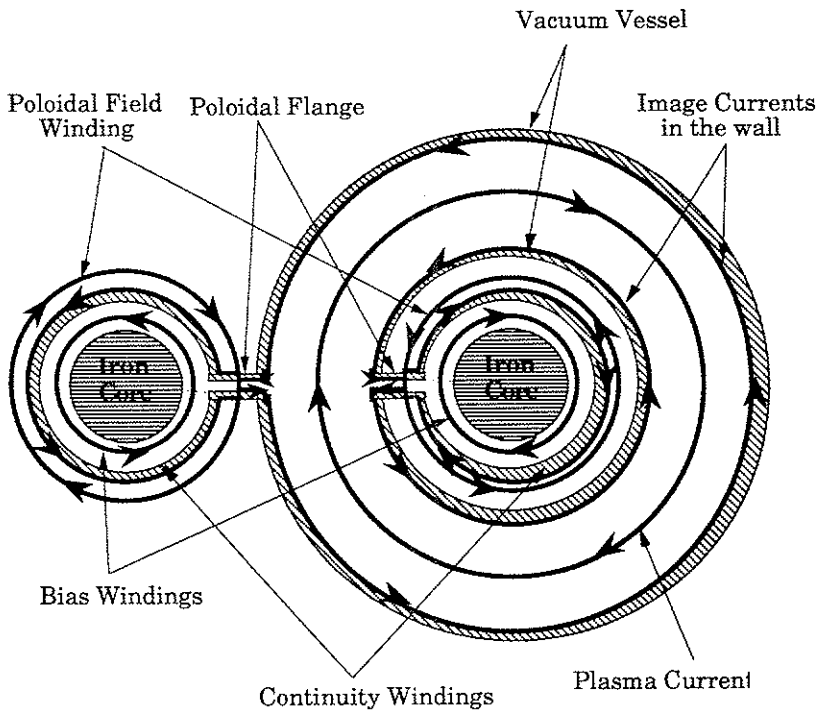

Figure 3.5 -- MST Poloidal Field System

Disassembly of the machine is greatly facilitated by the fact that there are no windings directly on the torus itself.

Rather than vacuum pumping through a few large holes which would cause significant field errors, pumping is accomplished through 198 1 1/2 inch diameter holes spread evenly around the bottom of the machine. The holes feed into a pumping duct which covers roughly two-thirds of the toroidal circumference. There are approximately 300 diagnostic portholes in the machine, which provide excellent diagnostic access; however, most holes are limited in size to 1 1/2 inches to minimize field errors.

The bare aluminum wall is exposed directly to the plasma. However, there are graphite rail limiters with a 1 cm radial extent at both toroidal gaps and the poloidal gap as well. The limiters scrape off the current in the edge region. The effective shadow of the limiters increases with increasing poloidal distance from the toroidal limiters. The toroidal limiters are the most important for scrape-off, as the current in the edge is primarily poloidal. The limiter shadow is important in edge probe work, as the plasma properties can be much different in the scrape-off-layer (SOL) than they are in the main current channel. Also, the poloidal variation in the radial extent of the SOL, due to the distance from the limiter must be considered in probe work.

Relative to other RFPs, the MST is large in size and medium in current.[10] The basic machine parameters and maximum global performance parameters are shown below in Table 3.1.[11,12] The parameters during the electrostatic fluctuation experiments will be given in the Chapter Five. The general diagnostics available on the machine are listed in Table 3.2.

Table 3.1--MST Parameters

major radius	1.5 m
minor radius	0.52 m
plasma current	0.6 MA
electron temperature	0.5 keV
ion temperature	0.4 keV
line-averaged density	1×10^{13} cm^{-3}
loop voltage	12 V
pulse length	80 msec
particle confinement time	~2 msec
energy confinement time	~1 msec

Table 3.2--MST Diagnostics

Diagnostic	**Purpose**
CO_2 laser interferometer	line-averaged density
Thomson scattering	electron temperature
various flux loops	magnetic flux
various Rogowski coils	current
edge electric probes	edge density and potential
edge magnetic coil array	magnetic field spectrum
soft x-ray array	soft x-ray activity
charge exchange analyzer	central ion temperature
visible light detector array	atomic emission
monochromator	Doppler line-broadening
Si(Li) detector	electron temperature

References

1 R. N. Dexter *et al.*, Fusion Tech. **19**, 131 (1991).

2 L. Woltjer, Proc. Nat. Acad. Sci. **44**, 489 (1958).

3 J. B. Taylor, Phys. Rev. Lett. **33**, 1139 (1974).

4 H. R. Strauss, Phys. Fluids **27**, 2580 (1984).

5 E. N. Parker, *Cosmical Magnetic Fields: Their Origin and Their Activity*, Clarendon, Oxford (1979).

6 E. J. Caramana, R. A. Nebel, D. D. Schnack, Phys. Fluids **26**, 1305 (1983).

7 K. L. Sidikman, *Ph. D. Thesis*, University of Wisconsin-Madison, 1990.

8 A. Almagri, *Ph. D. Thesis*, University of Wisconsin-Madison, 1990.

9 Y. L. Ho, *Ph. D. Thesis*, University of Wisconsin-Madison, 1989.

10 S. C. Prager, Plasma Phys. Controlled Fusion **32**, 903 (1990).

11 T. Rempel, A. Almagri, S. Assadi, J. Beckstead, R. Dexter, D. Den Hartog, G. Chartas, S. Hokin, T. Lovell, S. Prager, J. Sarff, E. Scime, W. Shen, C. Spragins, J. Sprott,F. Venneri, IEEE Int. Conf. on Plasma Science, Oakland (1990).

12 S. Hokin, A. Almagri, S. Assadi, J. Beckstead, G. Chartas, N. Crocker, M. Cudzinovic, D. Den Hartog, R. Dexter, D. Holly, S. Prager, T. Rempel, J. Sarff, E. Scime, W. Shen, C. Spragins, C. Sprott, G. Starr, M. Stoneking, and C. Watts, Phys. Fluids B **3**(8), 2241 (1991).

Chapter Four

Experimental Considerations of Fluctuation Measurements

A. Langmuir Probe Theory

1. Simple Probe Theory

A Langmuir probe is conceptually simple; a biased conductor with some known impedance to ground immersed in a plasma. The specific type of probe is determined by the voltage, impedance, and number of conductors. While the concept is straightforward, an exact interpretation of the results is prohibitively difficult. For this reason, approximations to an exact analysis must be made.

A probe immersed in a plasma will draw a current as a function of its bias voltage approximately as shown in Figure 4.1. As is shown in the figure, the current to the probe saturates at both negative and positive bias. In electron saturation, an electron sheath forms around the positively biased probe which effectively shields the potential from the surrounding plasma. The current drawn to the probe is then due to the random thermal motion of electrons impinging on the sheath and then being accelerated to the probe tip. In ion saturation, the phenomenon is the reverse. The electrons move faster, however; therefore, the electron saturation current has a larger magnitude.

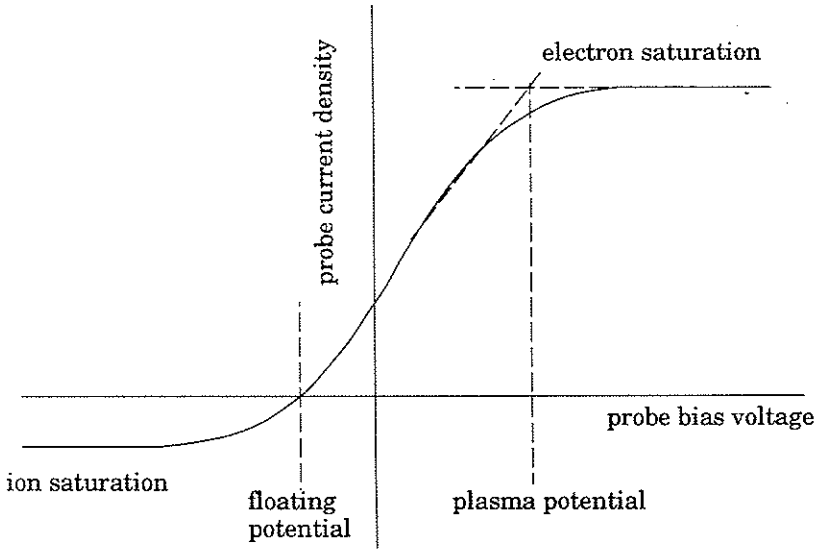

Figure 4.1 -- Langmuir probe bias curve.

When the probe is at the same potential as the background plasma, the current to the probe is again due to the random thermal motions of the charged particles and consists mostly of electrons due to their larger thermal velocity. For a probe to draw no net current, the probe must be at a potential which is negative relative to the plasma potential in order to repel the electron current except that amount which just balances the ion current. This potential, which is that assumed by an isolated conductor placed in the plasma, is known as the floating potential.

In a Maxwellian plasma with $T_i \leq T_e$, the curve between the

saturation regions is given by:

$$I = J^e_{sat} A_e \exp [(V_p - \Phi_{pl}) / T_e] - J^i_{sat} A_i \qquad (4.1)$$

where V_p is the probe voltage, Φ_{pl} is the plasma potential, A_i and A_e are the ion and electron collecting areas, respectively, and J^i_{sat} and J^e_{sat} are the ion and electron saturation currents, respectively.

The edge of the plasma sheath is essentially a boundary between the bulk plasma which has no dc electric fields and the region around the biased probe tip in which strong fields may exist. In order to ensure a smooth transition through the sheath edge, the electric field of the sheath and its derivatives must vanish there. This condition is found to impose a criterion on the velocity distribution of the particles collected at the probe tip. In the case of ion collection in which the electrons are Maxwellian and the ions have essentially zero temperature, solution of Poisson's equation with the boundary conditions satisfied yields the Bohm[2] criterion for the velocity of the ions at the sheath edge (where M_i is the ion mass):

$$v_i \geq \sqrt{\frac{T_e}{M_i}} \qquad (4.2)$$

which for this case is simply the ion acoustic velocity. In the case of finite ion temperature, $T_i + T_e$ is often used in place of T_e.[3] The Bohm criterion in effect states that the probe potential is not completely shielded from the plasma (when the colder species is collected) and that an electric field outside the sheath must be present to accelerate the ions up to the acoustic speed. The region outside the sheath in which this potential drop occurs is called the presheath.

In the case of monoenergetic ions, an approximate solution utilizing the construct of a sheath edge is:

$$J_{sat} = \frac{n_o}{2} v_i = \frac{n_o}{2}\sqrt{\frac{2T_e}{M_i}} \qquad (T_i=T_e) \qquad (4.3)$$

where n_o is the the bulk plasma density. This result is logical in that the current density collected by the probe would be equal to the density times the velocity at the sheath edge. The leading factor of 1/2 is due to the fact that satisfying Poisson's equation in the presheath, which is quasineutral, requires that the density drop by roughly a factor of two in order to sustain the potential drop of approximately $T_e/2$ there. Calculations by Laframboise[4] indicate, however, for the conditions of the present experiment, Debye length << probe radius << collision mean free path, that J_{sat} should be scaled as follows:

$$J_{sat} = \sqrt{\frac{2}{\pi}}\, n_o \sqrt{\frac{T_e}{M_i}} \qquad (4.4)$$

This result will be utilized in the data analysis that follows.

When the probe is collecting no net current (floating), the potential drop through the sheath may be determined by equating the expressions for the ion and electron current entering the sheath:

$$A_i n_s v_i = \frac{A_e n_s}{4}\sqrt{\frac{8T_e}{\pi m_e}} \exp\left(\frac{\Delta V}{T_e}\right) \rightarrow \frac{\Delta V}{T_e} = -2.84 \qquad (4.5)$$

where n_s is the density at the sheath edge and we have taken A_i and A_e to be equal. This potential drop combined with the presheath drop of about 0.5 T_e is then the difference between the plasma potential and the floating potential, i.e., $\alpha = -3.3 \rightarrow \Phi_{float} = \Phi_{plasma} - 3.3\, T_e$.

In the operation of a J_{sat} double probe, two probe tips are inserted into the plasma and biased with respect to one another, with the pair

electrically floating. The assumption is that the same characteristic curve applies to both probe tips, which are necessarily closely spaced. If the bias applied is much greater than the electron temperature, then the more negatively biased tip will draw ion saturation current. The other tip then must draw an equal electron current. This electron-collecting tip is only slightly more positive than the floating potential due to the steepness of the characteristic curve at that point (i.e, only a slightly positive voltage relative to the floating potential is required to draw an electron current equal to the ion saturation current). If the plasma is indeed Maxwellian, then the portion of the characteristic curve between the floating potential and the potential of the electron-collecting tip is Maxwellian. The difference between the voltage of the electron-collecting tip and a third, floating tip placed in the plasma is then proportional to T_e. Solving equation 4.1 for the three tips of the triple probe yields the following expression for T_e:

$$T_e\,(eV) = \frac{V_e - V_f}{\ln \frac{A_i + A_e}{A_f}} \qquad (4.6)$$

where V_e and V_f are the voltages of the electron-collecting tip of the double probe and the floating probe, respectively. In the case of equal areas, the denominator reduces to simply ln 2. This technique is known as the triple probe[5] method for measurement of electron temperature.

2. Corrections to Simple Probe Theory

One obvious correction to the simple theory for fusion plasmas is to

consider the effects of a magnetic field on the interpretation of probe data.[1] The primary effect of the magnetic field is to cause the charged particles to move in gyro-orbits about the magnetic field lines. For temperatures of 50 eV, and magnetic fields of 1 kG, cyclotron radii of 1.4 cm and 0.03 cm, respectively, for ions and electrons are obtained. For probe dimensions small compared to the cyclotron radii, there is little effect on collected currents. For the probes used in the electrostatic fluctuation work, the dimensions are large compared to the electron cyclotron radius and small compared to the ion cyclotron radius. The magnetic field will then have an effect on the electron saturation current, which is not of interest here, and on the magnitude of the sheath drop calculated in Equation 4.5, which is of interest here. The magnetic field will limit the effective electron-collecting area of the probe to surfaces normal to the magnetic field. For a cylindrical probe, the sheath drop magnitude is reduced to 2.39.

$$(2\pi r_p l_p)\, n_s v_i = \frac{(4\pi r_p l_p)}{4}\, n_s \sqrt{\frac{8T_e}{\pi m_e}}\, \exp\left(\frac{\Delta V}{T_e}\right) \rightarrow \frac{\Delta V}{T_e} = -2.39 \qquad (4.7)$$

Another factor which can affect the sheath drop is that of secondary electron emission due to electrons at the bulk temperature striking the probe. For a typical averaged value of the emission coefficient, γ_e, of 0.4, the sheath drop is reduced further by a factor of $\ln [1/(1-\gamma_e)] = 0.51$.[6] Ion saturation current is not strongly affected as the substantial negative bias inhibits electron collection.

Thermionic and secondary electron emission caused by nonthermal edge electrons, known to exist in MST and other RFPs, can also

complicate the determination of the various coefficients used in interpretation of the probe data. Estimates of this effect have been made by Rempel,[7] using a hot-electron secondary-emission coefficient of ~1.3 and allowing for possible space-charge limitations on this emission. For average hot-electron temperatures of 10 - 20 times the thermal edge electron temperature and densities 2% to 3% of the background plasma density, the resulting error is $\leq 25\%$ in α, $\leq 10\%$ in the coefficient in Equation 4.6, and $< 20\%$ in the coefficient in Equation 4.4.

The final correction to simple theory we will consider is that of sheath expansion. The effective collecting area of the probe is determined not by the area of the probe tip, but by the outside area of the plasma sheath. As the thickness of the sheath expands with the applied bias, the effective collecting area of the probe tip also expands. The sheath thickness is given approximately by $t_s = \left[\left(\Phi_{plasma} - V_{probe}\right)/T_e\right] \lambda_D$ for the case of the plasma potential more positive than the probe potential, which is the case for all tips in the triple probe. The effective radius is then $r_{eff} = r_p + t_s$. Utilizing $V_{bias} = V_i - V_e$ and $(V_f - \Phi_{pl})/T_e = \alpha$ and approximating $(V_e - \Phi_f)/T_e = 1$, we obtain the following expression for the effective radius of the ion collecting tip:

$$r_{eff} = r_p\left[1 + \frac{\lambda_D}{r_p}\left(-\alpha - 1 - \frac{V_{bias}}{T_e}\right)\right] \qquad (4.8)$$

Note that both α and V_{bias} are negative numbers here. Calculations by Laframboise[4] indicate that better fits are obtained when the coefficient of r_p is raised to the 2/3 power.

Sheath expansion can have a direct effect on temperature measurements, since each probe tip in the triple probe has a different voltage. Utilizing Equation 4.8 in Equation 4.6 for the temperature, we obtain:

$$\frac{V_e - V_f}{T_e} = \ln\frac{A_i + A_e}{A_f} = \ln\left[\frac{\left(1+\frac{\lambda_D}{r_p}\left(-\alpha-1-\frac{V_{bias}}{T_e}\right)\right)^{2/3} + \left(1+\frac{\lambda_D}{r_p}(-\alpha-1)\right)^{2/3}}{\left(1+\frac{\lambda_D}{r_p}(-\alpha)\right)^{2/3}}\right] \quad (4.9)$$

This equation must be solved iteratively, since the Debye length depends on the measured temperature and density. The iteration is performed computationally in a program written by Rempel.[6] For the data presented in the next chapter, the triple probe calibration factor was found to be 1.0 to 1.25, as compared to the equal-area, ideal, value of 1.4. The sheath drop for the floating probe is also affected by sheath expansion, with the effect being to decrease the magnitude of the drop by about 0.4.

If we add all the aforementioned effects, then we obtain a value for the sheath drop to a floating probe of $\alpha \equiv -2$:

-2.84 - 0.5 (presheath) + 0.45 (magnetic field) + 0.51 (secondary electrons) + 0.4 (sheath expansion) $\equiv -2$. This value for α is then used to calculate the plasma potential from the floating potential and the temperature as per Equation 2.6.

B. Experimental Description

1. Probe Description and Considerations

The probes used in the electrostatic fluctuation work consist of six tips, which are in two triplets separated by 11.4 mm as shown in Figure 4.2. Each of the two triplets operates independently as a triple probe. Two triplets are used to obtain gradients of the measured quantities. The probe tips themselves are 0.020" diameter tungsten wire with the tips of each triplet imbedded in an alumina stalk with four coaxial holes in a square arrangement. The tips in each triplet are separated by 1.6 mm, with each tip having an exposed length of 3 mm. Each alumina stalk is surrounded by a boron nitride sleeve, and both triplets are mounted in a one inch graphite head. The probe head is mounted on a 3/8" stainless steel stalk. Uncertainties in measurement of the tip sizes translate to an uncertainty in the tip area of approximately 10%.

Probe tip size is limited principally by three constraints.[1] The radius of the tip should be small compared to the ion cyclotron radius and large compared to the electron cyclotron radius. Additionally, the radius of the probe tip should be much greater than the Debye length. For the probes used on MST, $r_p/\lambda_D \sim 10$, therefore, sheath expansion effects are important, as discussed in the previous section.

Probe tip spacing is limited by several constraints, as well. The most

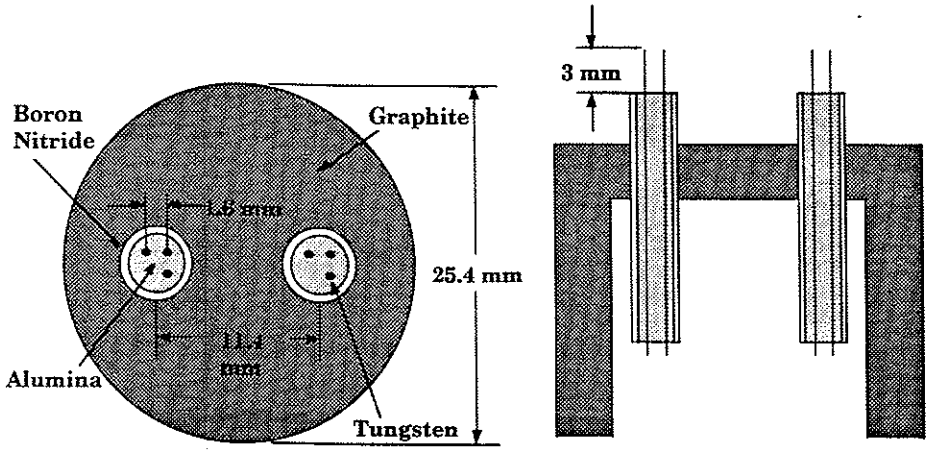

Figure 4.2 -- Schematic of Langmuir probe used for electrostatic fluctuation experiments.

obvious requirement is that the tip spacing be much greater than the Debye length. For measurement of fluctuating quantities, however, additional constraints regarding the spacing of the two triplets also come into play.[8] First, the spacing must be smaller than the smallest wavelength of the measured fluctuations, or else spatial aliasing will occur. The spacing must also be smaller than the coherence length of the frequency of fluctuations of interest in order to obtain a meaningful phase spectrum. Additionally, the spacing must be large enough that the maximum wavelength of the fluctuations not be greater than the accuracy of the measuring equipment, i.e., the minimum phase shift resolvable by the diagnostics must be greater than the minimum phase shift resulting from the fluctuations.

2. Electronics Description and Considerations

A block diagram of the experimental setup is shown in Figure 4.3. The probe is inserted through the wall of the vessel via a double o-ring probe lock with its outer stainless steel casing grounded to the vessel. The grounding of the various components is extremely important, since ground loops can cause serious noise pick-up and damaging stray voltages. The toroidal vessel is at building ground with a single ground strap connecting the vessel to the CAMAC crate. The CAMAC crate is connected to the computer via a fiber optic link. Machine ground is carried from the probe stalk to the chassis of the probe circuitry box via the shield of only one of the coaxial cables coming from the probe tips. The outputs of the probe circuitry box are, however, isolated from the chassis via isolated BNCs and obtain their ground through the AM502 crate which is grounded via the shields of the twisted bunch of coaxial cables going to the CAMAC crate. With this configuration, each component then obtains its ground through a single path. The circuit diagram for the probe electronics is shown below in Figure 4.4. The majority of the circuit is dedicated to supplying the appropriate bias for the J_{sat} double probe. The two tips labeled "ions" and "electrons" are the ion and electron collecting tips of the J_{sat} double probe. The bias is supplied by the lower part of the circuit diagram in which 4500μF of capacitance can be charged to a maximum of about 400V. A few seconds before the plasma pulse the connection between the capacitor bank and

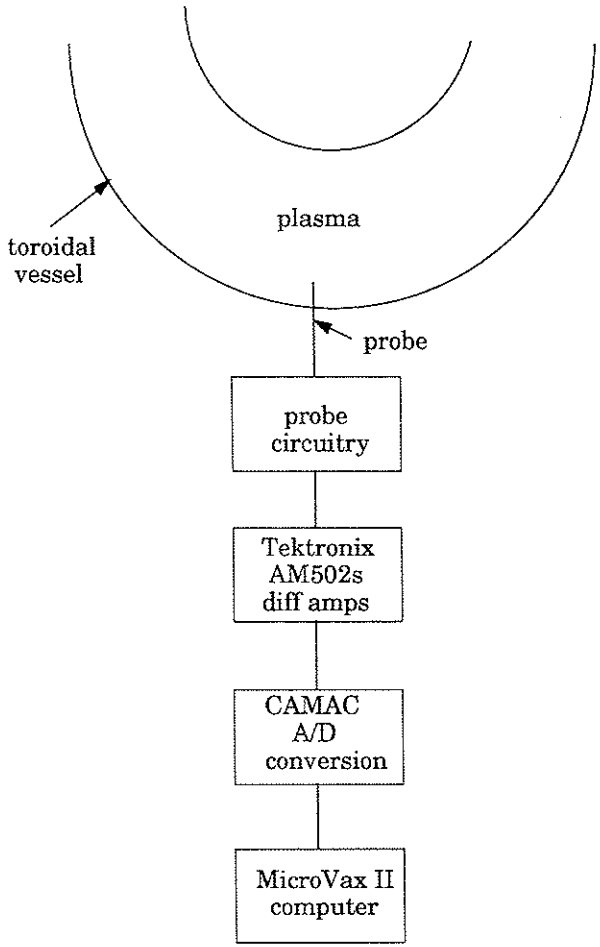

Figure 4.3 -- Block diagram of experimental setup.

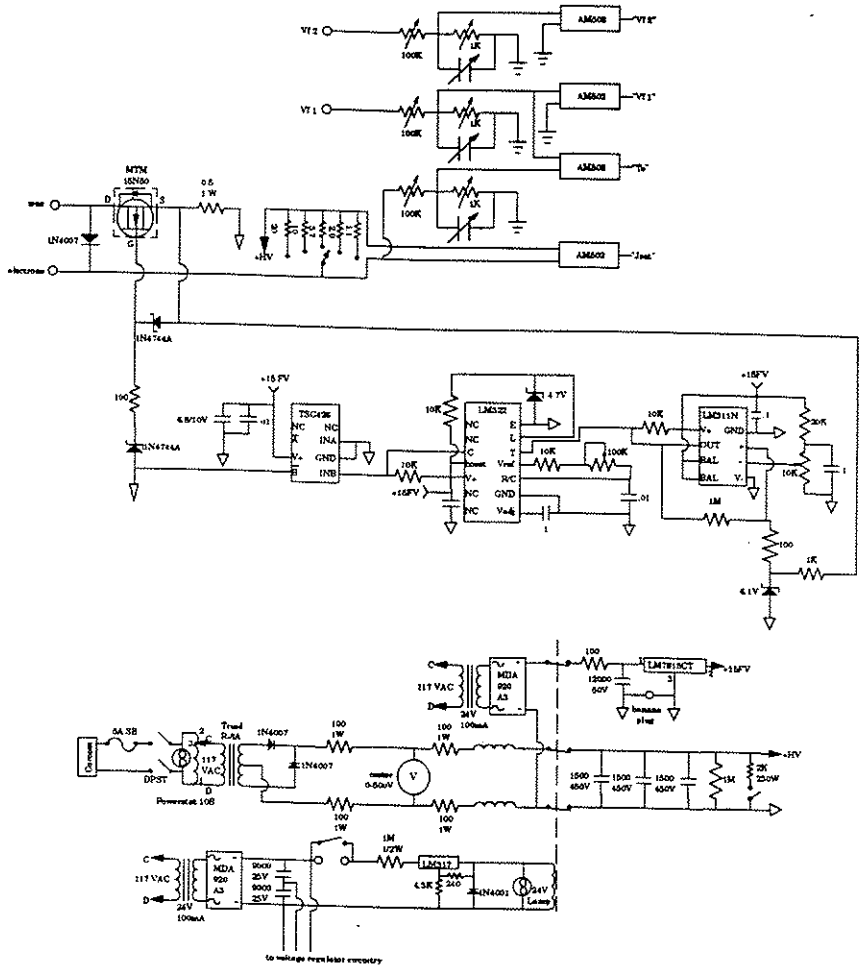

Figure 4.4 -- Circuit diagram for probe electronics.

the charging circuit is opened, thus allowing the bias source to float at the plasma's floating potential. The ion saturation current is then read as a voltage drop across the selected resistor.

The power MOSFET and the IC circuitry in the center of the diagram serve as current-limiting circuitry for the J_{sat} probe which was added retrospectively when it was observed that occasional arcing of the probe could lead to excessive damage to the circuit. When the current exceeds a certain value, the FET shuts off and does not allow current to flow. The current limit of up to about 10 amps and the off-time of up to 1.1ms are adjustable via the two potentiometers in the circuit.

The digitizers used in the system have a maximum input signal level range of -5 to +5 volts, therefore the input signals must be made to fall within that range. For signals with dc levels, supplying a dc offset to the signal in order to utilize fully the available voltage range is desirable. The signals each go through Tektronix AM502 differential amplifiers which have the option of providing a dc offset as well as low and/or high frequency roll-off and differential amplification.

The J_{sat} signal has a raw magnitude of less than 10 volts typically for the plasmas studied and J_{sat} resistor values used, and therefore does not need to be divided before going to the AM502. In fact, the gain is frequently increased somewhat with the AM502 in order to obtain the desired ~10V maximum signal. The other three signals, the two floating potentials and the signal proportional to T_e, however, are large and must be divided. The three voltage dividers are each set equally

with a voltmeter to divide by approximately 100. Lastly, a frequency-swept signal is input into the circuit to adjust the variable capacitors which compensate for unequal capacitances to ground, in order to minimize the relative phase shifts with frequency between signals.

The high-frequency roll-off provided by the AM502 differential amplifiers is not particularly sharp, therefore, with the 3 dB point set at 300 kHz, data digitization at a frequency of at least 1 MHz is needed to insure that no frequency aliasing occurs. This frequency is also necessary from the point of view of the two-point mode spectra measurements with the closely spaced probe tips used. For the case of very turbulent modes with large σ/k, where σ is the spectral width, the wave can pass too quickly by the second tip for the coherent structure to be detected if the digitization rate is too low.

C. Data Analysis [8]

1. Data Selection and Preliminary Analysis

After digitization, the signals are stored as vectors along with their corresponding time vectors by the MDS (Module Data System) data acquisition software. The analysis of the data is then carried out using the IDL (Interactive Data Language) software package. Ensemble averages are performed by taking small slices of the signals in time which are phenomenologically equivalent, referred to as "realizations"

and averaging them. The realizations must be chosen with care. Typically, the realizations are taken only within roughly ±10% of the peak plasma current when the bulk plasma parameters are relatively constant. Realizations which exhibit sawteeth are omitted, since the electrostatic probe signals exhibit large bursts at these times. Also, realizations in which the signals of interest have arcs or are saturated are also omitted from the ensemble. The duration of the realizations is generally 512 points, which is about 0.5 msec at a 1 MHz digitization rate. The realizations should be longer than the correlation time of the turbulence, which is generally not a problem unless there is a strong coherent mode. For a given amount of data, however, the larger the number of realizations, the better the statistics, therefore; the realizations should not be too long. We have found 512 points to be a good compromise for the electrostatic turbulence data.

The data acquisition software has the capacity to store relevant scalar parameters such as gains, variable resistor values, probe position, etc., in the database during each shot. These parameters are called "thumbwheels" and are stored in the computer by name and number. The descriptive names and values are entered into the computer via a routine designed for that purpose and may be changed easily from shot to shot. During data analysis, the values for a given shot may be recalled by name or number.

Preliminary analysis of the data involves first selecting the realizations as described above and storing them as vectors. Next, each vector is multiplied or divided by the relevant gains and other

parameters to convert it to its proper magnitude and units. The dc (mean) value of the signal for each realization is obtained by summing all points and dividing by the total number of points. Subtracting the mean from each point in the vector constitutes a zeroth order trend subtraction. A first order trend subtraction takes into account the overall linear slope of the realization in time. In order to perform this subtraction, we create a vector, **f**, with the same number of points as the realization, which is linear with the same slope as the realization and subtract it. If we label the points from zero to N-1, then the i^{th} point is given by: $f_i = x_0 - i\left(\frac{x_0 - x_{N-1}}{N-1}\right)$ where x_0 and x_{N-1} are the value of the first and last data points in the realization, respectively, and N is the total number of points in the realization.

Ideally, the realizations would be infinitely long, however, they are not and they are chopped off sharply at each end. This abrupt cut-off can cause the high frequency components of the data to be artificially large, and this effect must be compensated. The compensation is accomplished by multiplying the realization by a "window" function, W, which deemphasizes the edges of the realization relative to the center parts in a smooth way. The window we use is called the "Hanning window" where the i^{th} point is given by: $w(i)_{Hanning} = \frac{1}{2}(1 - \cos\frac{2\pi i}{N-1})$, with i = 0 to N-1. This window should only be used on vectors with zero mean, which in this case is ensured by the earlier trend subtractions. We can imagine a straight chopping out of the realization as effectively a rectangular window.

factor, as discussed in the section on preliminary analysis.

After performing the appropriate integration and normalization, the square root of the resultant number, expressed as a percentage, is then the number which is often loosely referred to as "$\frac{\tilde{n}}{n}$".

A quantity of fundamental importance in the study of turbulence is the *squared coherence* given by:

$$\gamma^2_{AB}(\omega) = \frac{\langle A(\omega)\, B(\omega)\rangle}{\left|\langle A^2(\omega)\rangle \langle B^2(\omega)\rangle\right|^{1/2}} \qquad (4.17)$$

where $\langle\rangle$ denotes an ensemble average. Statistically speaking, the coherence is a measure of the degree of linear correlation (or linear relationship) between two turbulent quantities as a function of frequency. Higher order coherences are a measure of the degree of nonlinear correlation. The coherence is, in general, a complex quantity, in which the phase represents the relative phases of the two fluctuating quantities. This phase can be used to calculate the wavenumber, k, as is indicated below. Also, electrostatic transport, as will be shown in the next section, is proportional to the coherence between two fluctuating quantities. The fluctuating quantities must not only have sufficient amplitude, but also be coherent, i.e., linearly correlated, in order to cause transport.

As was touched upon in Chapter One, the turbulence in the plasma is inherently nonlinear; therefore, there are no dispersion relations to describe the phenomena. Rather, each ω has a distribution of wavenumbers, k, associated with it. A useful characterization of the turbulence, then, is the ensemble-averaged distribution of power in (ω,k) space. This distribution is called the mode spectrum or spectral density, $S(\omega,k)$.[9]

The phase divided by the separation distance, Δx, between two closely spaced probe tips measuring the same quantity yields the local wavenumber, k. Explicitly:

$$k(\omega) = \frac{\tan^{-1}\left(\frac{\mathrm{Im}(H)}{\mathrm{Re}(H)}\right)}{\Delta x}, \quad \text{where } H(\Delta x,\omega) = \frac{1}{N}\Phi^*(x,\omega)\,\Phi(x+\Delta x,\omega) \qquad (4.18)$$

where N is the number of points in the realization and Φ is the FFT of the signal of interest, e.g., the floating potential. If the two tips are poloidally spaced, then a poloidal k is obtained and analogously for toroidal k. The poloidal mode number is then $m=k_p a$ and the toroidal mode number is $n=k_t R_0$.

In order to calculate S, for each value of ω in each ensemble term, the value of k is calculated and the fluctuation power at that point is added to the appropriate bin in (ω,k) space. Repetition of this process for each realization pair then produces a reconstruction of the mode spectrum.

This two-point method cannot be used to calculate wave numbers larger than $\pm\pi/\Delta x$, as was noted in the probe description section of this chapter. The spectrum decaying sufficiently at the maximum measurable k values indicates that no spatial aliasing is occuring.

3. Electrostatic Fluctuation Induced Transport

We have, from Equation 2.2, $\tilde{v} = \frac{\tilde{E} \times B}{B^2}$, where we need to measure the fluctuating velocity in order to determine the transport coefficients for particles and energy. Therefore, we use $\tilde{v}_r = -\frac{\tilde{E}_t}{B_p}$ and we find that the other term involving E_p ($<< E_t$) and B_t ($<< B_p$) contributes less than 1% to the measured flux. A positive number for v_r then indicates a radial velocity directed *outward*.

The coordinate system convention used in the calculations is shown in Figure 4.5, where $\hat{\vartheta}$ is the poloidal direction, $\hat{z}$ is the toroidal direction, and $\hat{r}$ is the radial direction.

We have $\tilde{E}_t = -\nabla_t \tilde{\Phi}_{plasma}$ which may be Fourier transformed as:

$$\tilde{E}_t(\mathbf{r}, t) \rightarrow -ik(f)\Phi(f)e^{i\mathbf{k}(f)\cdot\mathbf{r}}$$

and written, with the use of Equation 2.7, as:

$$\tilde{E}_t(f) = -ik_{\Phi_f}(f)\,\tilde{\Phi}_f(f) + i\alpha k_{T_e}(f)\,\tilde{T}_e(f) \qquad (4.19)$$

where k_{Φ_f} and k_{T_e} are the waveneumbers for fluctuations in floating potential and electron temperature, respectively, in the toroidal direction.

The wavenumber, k, must be obtained in such a way that the sign convention is consistent with the gradient operator, as defined by our coordinate system. We have, for two spatially separated measurements of a signal ϕ: $k\Delta x$ = phase $\left[\phi_1^* \phi_2\right]$ = phase (ϕ_2) - phase (ϕ_1). If k>0, then ϕ_2 leads ϕ_1, i.e., the vector **k** is pointing from 1 to 2. Therefore, for consistency with the coordinate system, the signal at a less positive value of the toroidal coordinate should be the one which is complex conjugated when the cross power between the two signals is computed. Obtaining the correct sign is critical in order to determine if the transport is inward or outward.

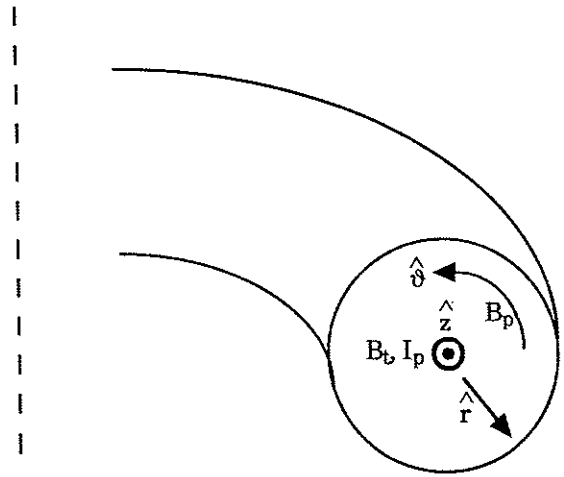

Figure 4.5 -- Coordinate system used for electrostatic transport calculations.

We have $\Gamma_p = \mathrm{Re}\left\langle \tilde{n}_e \tilde{v}_r^* \right\rangle$, where $\mathrm{Re}\,(\tilde{n}_e^* \tilde{v}_r) = \mathrm{Re}\,(\tilde{n}_e \tilde{v}_r^*)$. Substituting in the above expressions for $\tilde{v}_r$ and $\tilde{E}_t$, we obtain:

$$\Gamma_p(f) = \frac{-1}{B_p}\,\mathrm{Im}\left[\left\langle \tilde{n}_e^*(f) k_\Phi(f) \tilde{\Phi}_f(f) \right\rangle - \alpha \left\langle \tilde{n}_e^*(f) k_\Phi(f) \tilde{T}_e(f) \right\rangle\right] \qquad (4.20)$$

Chapter Five

Experimental Results

A. Experimental Parameters

The typical, optimized, parameters for the MST reversed field pinch are listed in Table 3.1. For the present experiment, however, considerably lower current, cooler plasmas were utilized. As the experiment involves physically inserting the probes into the plasma, the survivability of the probes is a real concern, as well as the corruption of the data by thermionic emission from overheating of the probes.

The plasma parameters of the present experiment [$I_p \leq 250$ kA, $\bar{n}_e = (0.6\text{-}0.8) \times 10^{13}$ cm^{-3}, $T_{e0} \leq 180$ eV], are shown in Figure 5.1. For these conditions, a single-turn loop voltage $V_l = 15.5$ V, pinch parameter $\Theta = B_p(a)/\langle B_t \rangle = 1.85$ (where $\langle B_t \rangle$ is the volume-averaged toroidal field), and reversal parameter $F = B_t(a)/\langle B_t \rangle = -0.15$ were obtained.

For the data presented, the probes were located at r = 48 to 51 cm (from 1 to 4 cm from the wall), 40° above the outer midplane, and 120° from the poloidal gap. Graphite toroidal rail limiters extend 1 cm from the wall of the vessel at the inner and outer midplane. Measurements made at other poloidal and toroidal locations indicated no major differences in the characteristics of the turbulence and resultant

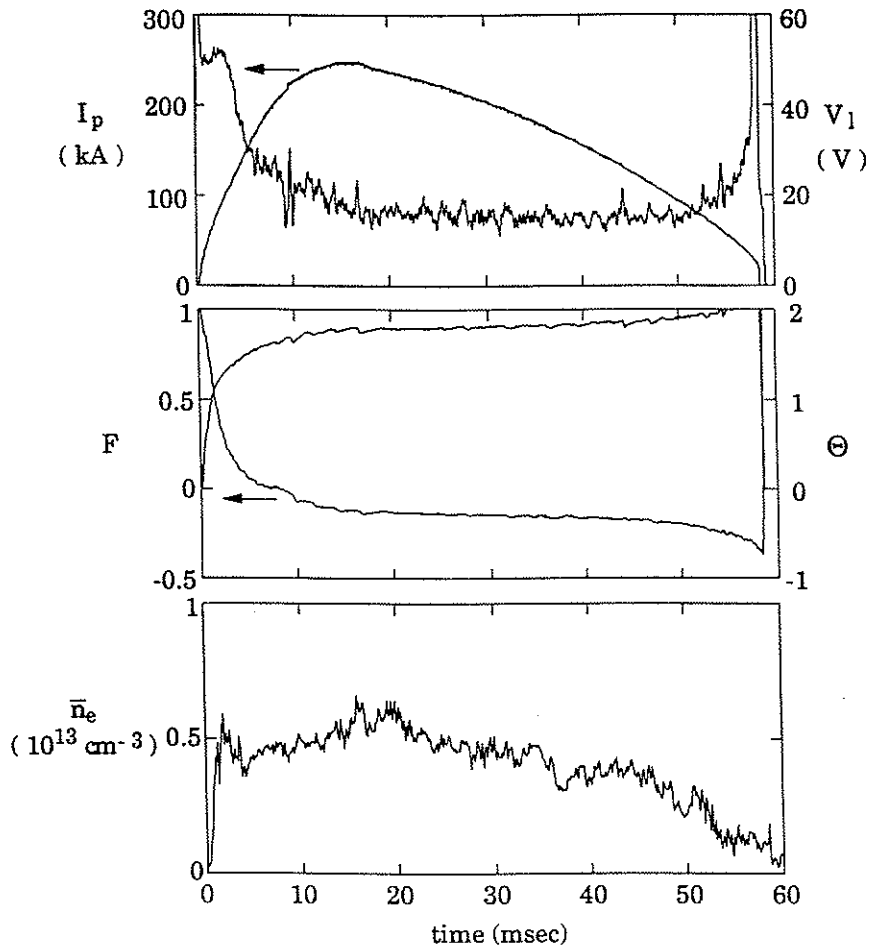

Figure 5.1 -- Waveforms of I_p *and* V_l, F *and* Θ, *and* $\bar{n}_e$.

transport. The only differences noted were in the proximity of the bulk plasma to the wall, presumably due to field errors.

B. Electrostatic Fluctuation Characteristics

Electrostatic fluctuations in the edge of MST are broadband and turbulent. Typical power spectra, shown in Figure 5.2, peak at low frequencies and fall monotonically with frequency. The radial profiles of the relative fluctuation amplitudes from 3-200 kHz, calculated using Equations 4.13, 4.15, and 4.16, are shown in Figures 5.3. The fluctuation amplitudes are large, with $|\tilde{n}_e| / n_e \sim 30\% - 55\%$ and $|\tilde{T}_e| / T_e \sim 15\% - 40\%$. The relative fluctuation levels increase with radius on average.

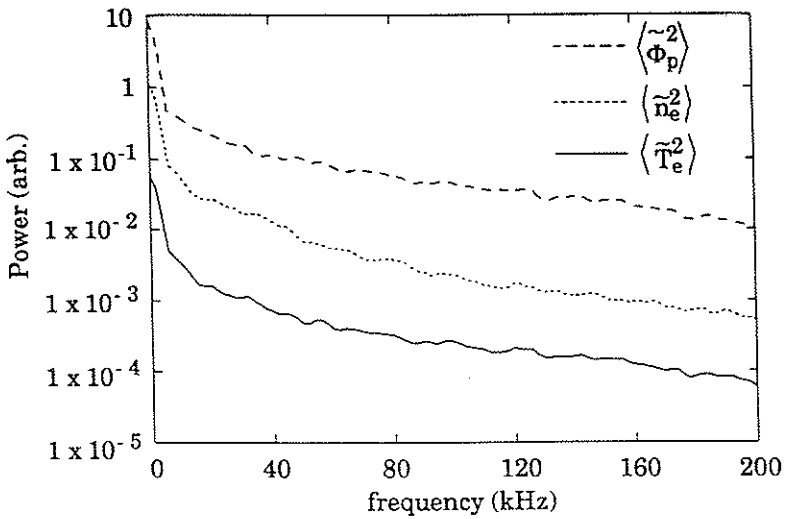

Figure 5.2 -- Fluctuation power spectra of $\tilde{\Phi}_p$, $\tilde{n}_e$, and $\tilde{T}_e$.

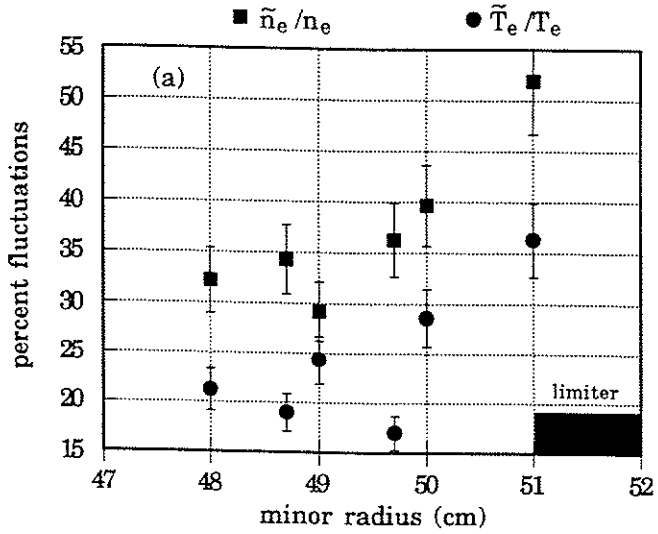

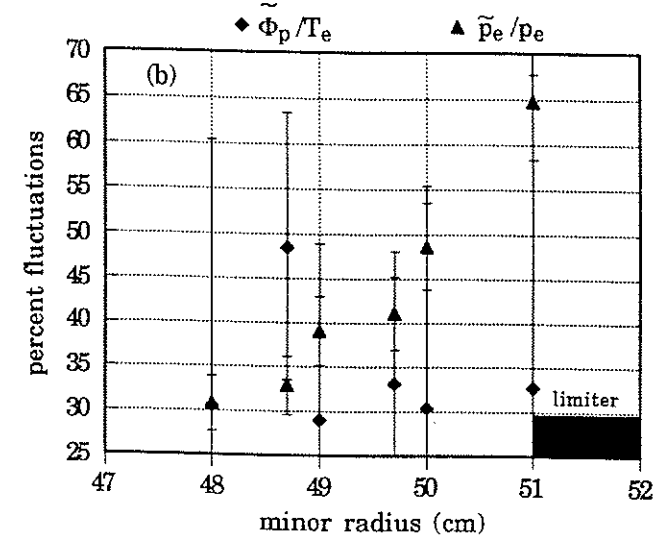

.3 -- Relative fluctuation amplitudes of (a) $\tilde{n}_e / n_e$, $\tilde{T}_e / T_e$ *and* , $\tilde{\Phi}_p / T_e$.

Pressure fluctuations are also large, with $|\tilde{p}_e|/p_e \sim 30\% - 65\%$. Plasma potential fluctuation amplitudes, $|\tilde{\Phi}_p|/T_e$ are, on average, relatively uniform, but have large error bars. Within uncertainties, we find no evidence that the Boltzmann relation for electrons is violated. The pressure gradient and electrostatic forces on the electrons appear to be in balance, i.e. $|\tilde{p}_e|/p_e \sim |\tilde{\Phi}_p|/T_e$, (Figure 5.3(b)).

The two-point spectral density, S(ω,k), has been measured for some of the fluctuating quantities. The spectrum for two poloidally separated

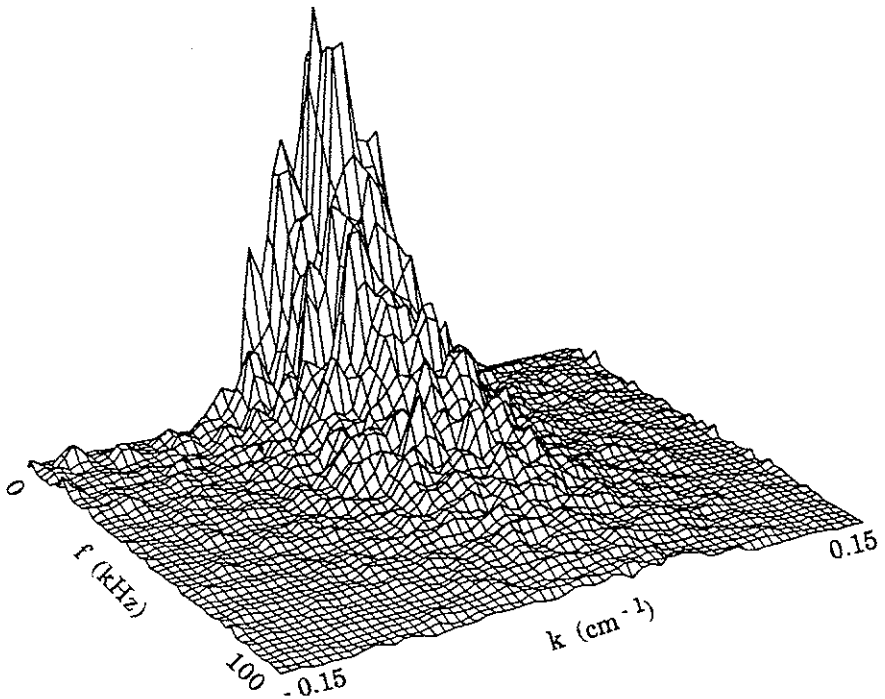

Figure 5.4 -- Poloidal S(k,ω) *for* $\tilde{\Phi}_f$.

probes measuring floating potential is shown in Figure 5.4. The power is greatest at low frequencies, near k=0 and broadens with increasing frequency. The k-spectra for particular frequency bands of the spectral density may be summed and converted to mode numbers to yield toroidal and poloidal mode number spectra for comparison to the magnetic fluctuation[1,2] spectra on MST. The resulting toroidal mode number spectra are shown in Figure 5.5 (with $n=k_\phi R$, where ϕ indicates the toroidal direction). At low frequencies (10-25 kHz), electrostatic n spectra are broad, with a width of $\Delta n \sim 70$ (Figures 5.5(a) and 5.5(b)). This observation is in contrast to the radial magnetic-field fluctuation n spectrum, which is dominated by a tearing mode peak at $n \sim 2R/a \sim 6$ and $\Delta n \leq 10$.

At higher frequencies (50-100 kHz), the electrostatic n spectra broaden even further to $\Delta n \sim 150$. At these frequencies, the n spectrum for $\tilde{\Phi}_f$ tends to peak in the ion drift direction at $n \sim 10\text{-}30$ ($k_\phi \rho_s \sim 0.05\text{-}0.15$, where $\rho_s \sim 0.8$ cm in the edge). Because of uncertainties in the phase-shift measurement, this value is at the limits of the diagnostic accuracy. The n spectrum for $\tilde{J}_{sat}$ shifts to the electron drift direction, peaking at $n \sim 10\text{-}40$. While the $\tilde{B}_r$ spectrum also shows a similar shift in this frequency band, the width is significantly smaller, $\Delta n \sim 60$.

Poloidal mode spectra for $\tilde{\Phi}_f$ (Figure 5.5(c)), obtained from measurements using two electrostatic probes separated by 19.8 cm, show a much narrower width. At low frequencies, the spectrum is centered at $m=1$ and has $\Delta m \sim 3$. The spectrum again broadens with

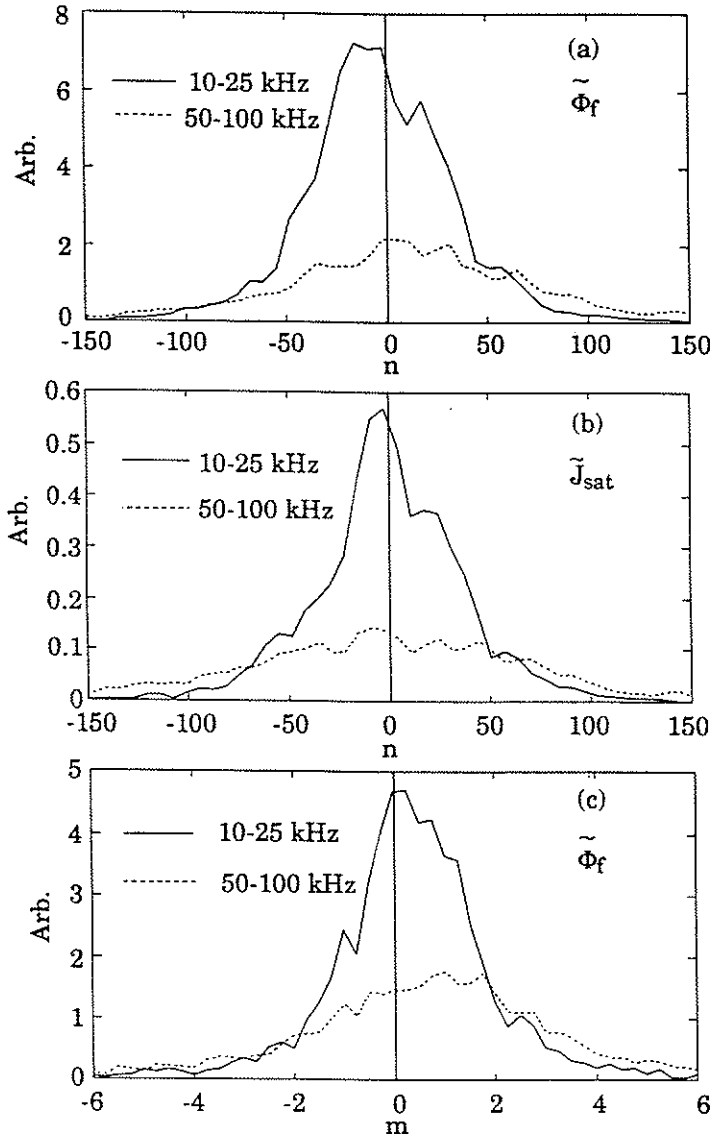

Figure 5.5 -- Low and high frequency m *spectra for (a)* $\tilde{\Phi}_f$, *and* n *spectra for (b)* $\tilde{\Phi}_f$, *and (c)* $\tilde{J}_{sat}$.

frequency, to a width of $\Delta m \sim 6$, peaked at m=1-2, at 50-100 kHz. While showing some general similarities to the electrostatic m spectra, the m spectra for $\tilde{B}_r$ are much more sharply peaked about m=1, especially at low frequencies where $\Delta m \sim 1$.

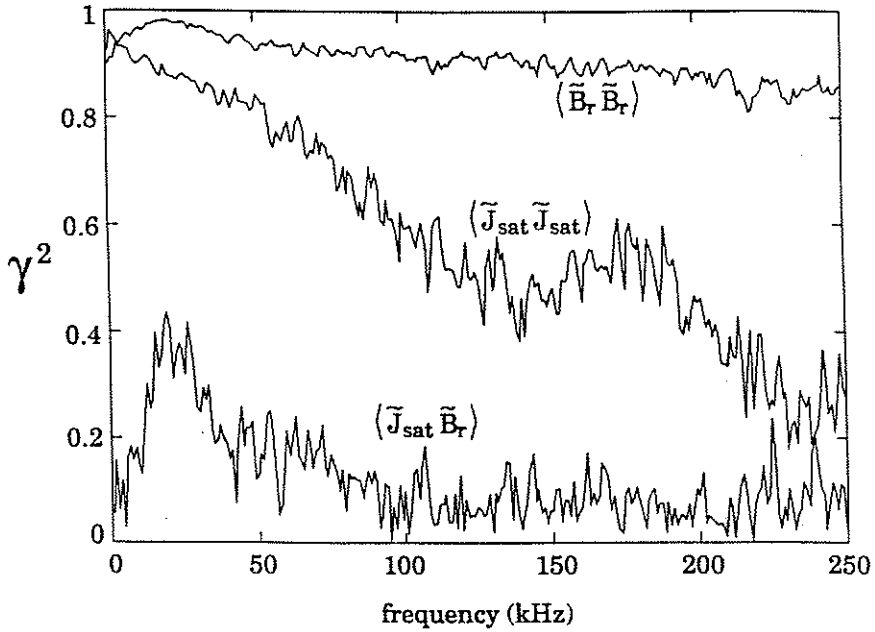

Figure 5.6 -- Squared coherence (γ^2) *of two* $\tilde{B}_r$ *and two* $\tilde{J}_{sat}$, *each separated toroidally by 1.8 cm, and between* $\tilde{J}_{sat}$ *and* $\tilde{B}_r$ *separated by 0.5 cm.*

limiters.

The separate contributions of $\langle \tilde{n}_e \tilde{v}_r \rangle$ and $\langle \tilde{T}_e \tilde{v}_r \rangle$ to the total electron energy flux spectrum at r = 48 cm are shown in Figure 5.7(b), and the total electron energy flux as a function of minor radius is shown in Figure 5.8(b). The global electron energy confinement time from electrostatic fluctuations has been calculated using Equation 4.23. When simple convection based on the first term in Equation 4.21 was assumed, and temperature fluctuation effects were ignored, an electron energy confinement time based on the flux at r = 48 cm of ~ 2 msec was obtained. However, temperature fluctuations add an inward energy flux, resulting in τ_E ~ 4 - 5 msec. This value is significantly larger than the global electron energy confinement time in MST of ~ 0.5 - 1 msec at low plasma currents.

References

1 A. Almagri *et al.*, "Edge Fluctuations in the MST Reversed Field Pinch," in the Proceedings of the Workshop on Physics of Alternative Confinement Schemes, Varenna, 1990 (to be published).

2 S. C. Prager, Plasma Phys. Controlled Fusion **32**, 903 (1990).

3 W. L. Rowan *et al.*, Nucl. Fusion **27**, 1105 (1987).

4 S. Hokin *et al.*, Phys. Fluids B **3**(8), 2241 (1991).

Chapter Six

Summary and Conclusions

Langmuir probes have been used to measure electrostatic fluctuations in the edge of a large reversed field pinch. The fluctuation amplitudes are large, with $|\tilde{n}_e|/n_e$ ~ 30% - 55%, and $|\tilde{T}_e|/T_e$ ~ 15% - 40%. Pressure fluctuations and plasma potential fluctuations are also large, with no significant evidence that force balance along the magnetic field is violated. The relative fluctuation amplitudes for density, temperature, and pressure are observed to increase with minor radius in the edge plasma.

The toroidal and poloidal mode spectra for the electrostatic signals have been measured and are found to be broad. The spectra are centered nearly at $m = 1$, $n = 0$, although some shift at higher frequency exists. This observation is in contrast to the observed radial magnetic-field fluctuation spectra. Consistent with this difference is the fact that the correlation between electrostatic ($\tilde{J}_{sat}$) and magnetic ($\tilde{B}_r$) fluctuations in the edge of MST is modest, and only exists at low frequencies.

The measured electrostatic fluctuation induced radial particle transport limits the particle confinement time to ~ 1 msec, which is comparable to the total particle confinement time. In contrast, the electrostatic energy flux is relatively small, contributing only ~20% to the observed global energy transport. In both instances, the temperature

fluctuations play an important role, contributing a relatively substantial inward flux of both particles and energy.

If one were to attribute transport in the RFP only to electrostatic and magnetic fluctuations, then these results would imply that magnetic fluctuations do not contribute substantially to particle transport. This result is sometimes anticipated to be the case, in view of the ambipolarity constraints for either localized modes or global tearing modes. However, the relatively large magnetic fluctuations might still drive significant energy transport.

Despite the geometric differences between the RFP, tokamak, and stellarator, there is a qualitative similarity in the amplitude and spectral breadth of edge electrostatic fluctuations in the three configurations. Moreover, it appears that edge energy transport in the RFP from electrostatic fluctuations alone might be of similar magnitude to the transport in a tokamak or stellarator of similar minor radius and plasma current (but higher magnetic field). Considered together, these ideas might imply that the relatively larger magnetic fluctuations in the RFP are responsible for the poorer observed energy confinement in these devices.